Two band transport and the question of a metal-insulator transition in GaAs/GaAlAs two dimensional holes

Yuval Yaish,* Oleg Prus, Evgeny Buchstab, Gidi Ben Yoseph, and Uri Sivan
Department of Physics and Solid State Institute, Technion-IIT, Haifa 32000, Israel

Iddo Ussishkin† and Ady Stern
Department of Condensed Matter Physics, The Weizmann Institute of Science, Rehovot 76100, Israel
(September 25, 2001)

The magnetotransport of two dimensional holes in a GaAs/AlGaAs heterostructure is studied experimentally and theoretically. Spin-orbit splitting of the heavy hole band is manifested at high carrier densities in two Shubnikov-de Haas frequencies, classical positive magnetoresistance, and weak antilocalization. The latter effect combined with inelastic scattering between the spin-orbit split bands lead to metallic characteristics, namely resistance increase with temperature. At lower densities, when splitting is smaller than the inverse elastic scattering time, the two bands effectively merge to yield the expected insulating characteristics and negative magnetoresistance due to weak localization and interaction corrections to the conductivity. The "metal to insulator" transition at intermediate densities is found to be a smooth crossover between the two regimes rather than a quantum phase transition. Two band calculations of conventional interference and interaction effects account well for the data in the whole parameter range.

I. INTRODUCTION

The study of magnetotransport in two dimensional (2D) electronic systems regained considerable interest since the observation of Kravchenko *et al.*[1] that the resistance of high mobility, high density silicon MOSFETs decreases and saturates to a residual value as the temperature is reduced. This metallic characteristic is in sharp contrast with the prevailing dogma that 2D systems are insulating[2] although interaction may possibly lead to delocalization.[3] The conflict between Ref. 1 and the expected insulating characteristics motivated extensive experimental and theoretical efforts. Soon, similar characteristics have been observed in other silicon samples,[4] SiGe quantum wells,[5] AlAs based 2D electron gas (2DEG),[6] 2DEG in GaAs/AlGaAs heterostructures,[7] 2DEG in GaAs with self assembled InAs quantum dots,[8] and various realizations of 2D hole gas (2DHG) in GaAs/AlGaAs heterostructures.[9,10,11,12]

The samples that show metallic characteristics share some other features:
(a) Insulating behavior at low carrier densities, namely, resistance increase with decreasing temperature.
(b) Weak dependance of the resistance upon temperature at some intermediate density (coined "metal-insulator transition" (MIT)).
(c) Negative magnetoresistance at the density corresponding to the MIT.
(d) Large, positive magnetoresistance for magnetic fields parallel to the layer.
(e) A crossover from metallic to insulating characteristics for large enough parallel magnetic fields.

The zero field crossover from metallic to insulating behavior was identified by some authors as a second order phase transition.[13,14,15] Scaling theory has been constructed[16] and even reentrant transition to an insulating phase, at still higher densities, has been argued to occur for holes in GaAs.[17]

Notwithstanding the remarkable similarities between the magnetoresistance and temperature/density dependences of the different material systems and samples listed above, some gross differences should be appreciated:
(i) While the weak field magnetoresistance in silicon samples is negative in all regimes, it is positive for holes in GaAs in most of the metallic regime (high carrier concentration).
(ii) While only single band is observed in silicon samples, the 2DHG in GaAs samples, in most of the metallic regime, is characterized by two distinct bands. These bands are manifested in two Shubnikov-de Haas (SdH) frequencies, as well as in classical, positive magnetoresistance.
(iii) The relative resistance change with temperature in different materials vary between about 1% for electrons in GaAs to an order of magnitude in silicon MOSFETs.
(iv) The "critical resistance" at the MIT varies substantially from sample to sample and between different material systems. In contrast to some early claims it can deviate substantially from one resistance quantum[18].
(v) The large effect of back gating in GaAs 2DHG[11,19] is absent for electrons in silicon[20] or is at least very different[21].

The extent to which the magnetotransport in different 2D systems is universal is hence unclear at this point. The multivalley band structure of silicon, the short range potential fluctuations in silicon as opposed to the long range ones in GaAs, the strong spin-orbit coupling in III-V materials, not to mention obvious differences in effective masses and Zeeman factors, might all turn out to be important.

A wide spectrum of mechanisms has been proposed to account for these features, including a new type of superconductivity,[13] a novel metallic phase induced

by disorder enhanced interactions[14] (this direction is based on the earlier works in Ref. 3), Wigner glass and non-Fermi liquid,[15] a new liquid phase,[22] impurity scattering,[23] temperature dependent screening,[24,25] spin effects,[21,26] interband scattering,[12] band structure effects,[11,19] and classical percolation.[27] None of these explanations account for all features in all materials. It would thus be fair to state that the metallic behavior, as well as the other features listed above, remain unexplained as universal phenomena.

The present manuscript presents an extensive experimental and theoretical study of magnetotransport in two dimensional hole gas in GaAs/GaAlAs heterostructures. The experimental data pertain to measurements of high mobility samples as well as low mobility ones. The data display all the characteristic features listed above. At high densities all samples display metallic characteristics (Figs. 3, 6c-e). At low densities the samples are insulating (Fig. 6a) in accordance with point (a) above (we have chosen to display the insulating data for the low mobility sample to avoid possible inhomogeneities that might occur at the very low densities where the high mobility samples turn insulating). At an intermediate density (Fig. 6b), the samples display weak dependence of the resistance upon temperature ("MIT", point (b) above). All samples are characterized by a large, positive magnetoresistance for a parallel magnetic field (points (d), (e) above and Fig. 7) and suppression of the metallic characteristics by such a field.

In a recent letter[12] we reported magnetotransport measurements done on a high mobility 2DHG sample. Concentrating on the high density regime we were able to show that the metallic characteristics result from inelastic scattering between the two heavy hole bands split by the spin-orbit interaction. The positive magnetoresistance observed in that sample was fully accounted for by the well known classical two band formulae[28,29,30] and the resistance increase with temperature was shown to result from the enhancement of Coulomb scattering between the two spin-orbit split bands. That work thus explained the metallic characteristics with well known semiconductor physics without invoking a novel metallic phase or any other "new" physics. The spin-orbit split bands were studied extensively both experimentally,[11,19,31,32,33] and theoretically.[34,35,36,37] In fact, Murzin *et al.*[38] have previously shown that interband Coulomb scattering is manifested in a resistance increase with temperature.

The present manuscript extends our previous work in several ways. First we refine the high density data analysis and show that the negative magnetoresistance at larger magnetic fields results from quantum corrections due to Coulomb interaction.[39,40,41] Next we report new measurements covering the insulating, MIT, and metallic (high density) regimes. The data conform with previous magnetotransport measurements on 2DHG.[9,10,11,19,32,38,42,43] Careful analysis then shows that well-known physics accounts for all data. The emerging picture is briefly as follows.

It is well known, both theoretically[34,35,36,37] and experimentally[11,12,19,31,32,33], that the bulk heavy hole band in assymmetric GaAs/AlGaAs heterostructures is split by spin-orbit interaction. The resulting sub-bands are manifested by two SdH frequencies, as well as by a classical, Lorentzian shaped, positive magnetoresistance (PMR). The band splitting energy, ϵ_g, vanishes at $k = 0$ and increases with k.[34] At low densities, when ϵ_g at the Fermi energy is small and the elastic scattering time, τ, is short, $\epsilon_g \ll \hbar/\tau$, the two bands are strongly mixed and spin-orbit splitting is unimportant. The resulting magnetoresistance is negative and dominated by weak localization (WL) and hole-hole Coulomb interaction. As the temperature is increased, these quantum corrections are suppressed and the sample becomes more conductive. At high densities, the sub-band splitting is large and τ is long, thus $\epsilon_g \gg \hbar/\tau$. The two sub-bands are hence distinguishable. The weak field magnetoresistance is positive and dominated by weak anti-localization (WAL) induced by inter sub-band scattering (effectively, spin-orbit scattering), hole-hole interaction (Altshuler-Aronov correction[39]), and classical two band magnetoresistance. A slightly higher magnetic field suppresses the quantum corrections in the Cooperon channel while the classical magnetoresistance persists. At still higher fields, the classical magnetoresistance is also suppressed and the magnetoresistance turns negative due to hole-hole interaction in the diffuson channel.

The metallic characteristic, $d\rho/dT > 0$, in the high density regime is traced to the enhancement of inelastic inter sub-band scattering as well as the suppression of quantum corrections (especially the WAL) with increased temperature. The weight of quantum corrections relative to the classical effect depends on sample resistivity. The quantum corrections are negligible in high mobility samples and very important in the low mobility ones close to the MIT. The weak temperature dependence of the resistivity at the MIT merely reflects effective cancellation of the resistance increase with temperature due to inelastic interband scattering and suppression of WAL, against resistance decrease with temperature due to the suppression of hole-hole interaction.

Our analysis thus explains how the sample crosses over from an insulator at low densities to a "metal" at higher densities. Moreover, we account for the change from negative to positive magnetoresistance as the density is increased. All these features emerge from the well known band structure of holes combined with conventional quantum corrections to the magnetoresistance. No new metallic phase is invoked.

The manuscript comprises the following parts. Section II provides a refined analysis of our previously published data[12] on high mobility samples. The refined analysis includes hole-hole interaction in the diffuson channel. The extracted inter and intraband scattering rates remain unchanged. The analysis provides new information about the Coulomb interaction parameter at different densities.

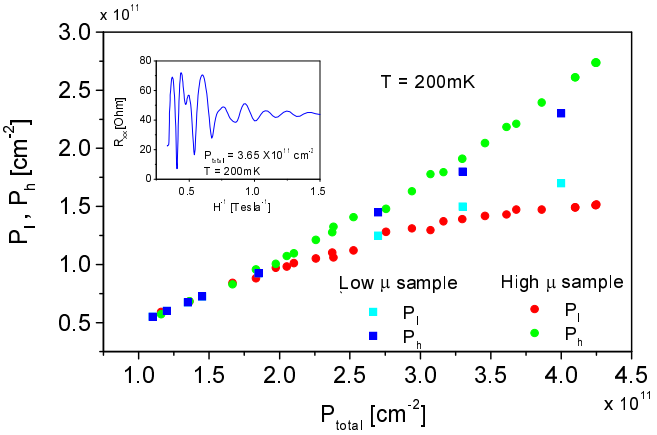

FIG. 1: Hole density in the light (p_l) and heavy (p_h) spin-orbit split bands as a function of total density. Inset - One of the Shubnikov de Haas traces (high mobility sample) used to determine the hole densities.

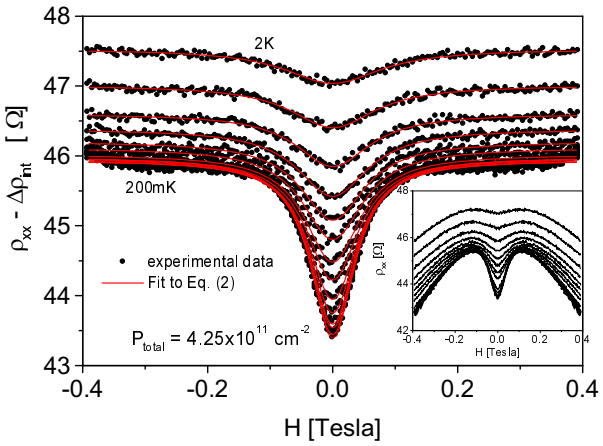

FIG. 2: The two-band classical contribution to the magnetoresistance for different temperatures (high mobility sample). Note the perfect Lorentzian shape MR at low fields. Inset- Full magnetoresistance curves for the same temperatures.

The theory of quantum corrections to the magnetotransport is briefly reviewed in Section II B. Previous calculations are extended to account for two sub-bands with different mobilities. Details of these calculations are provided in the Appendix. Extensive data measured on a lower mobility sample are provided in section III. The data are analyzed taking into account WL, WAL, hole-hole interaction in the cooperon and diffuson channels, and interband scattering. A comprehensive picture of magnetotransport in a 2DHG is compiled in section IV. Section V details some theoretical aspects of magnetotransport in a two band system with spin-orbit splitting. Plasmon mediated Coulomb scattering is analyzed in this section, and shown to yield an Arrhenius temperature dependence. Finally, this section also discusses the quantum corrections to the magneto-conductivity in this system.

II. HIGH MOBILITY 2DHG SAMPLE AND THEORETICAL BACKGROUND

A. Experiment

The high mobility sample had a mobility of $\simeq 300,000\ \mathrm{cm}^2/(\mathrm{V\,s})$ at $p = 4\times10^{11}\ \mathrm{cm}^{-2}$ and $T = 200$ mK. The low mobility sample had a $\simeq 20,000\ \mathrm{cm}^2/(\mathrm{V\,s})$ mobility at a similar carrier density and $T = 400$ mK. The 2DHG was confined in both samples to a GaAs/$Al_{0.8}Ga_{0.2}$As interface in the $\langle 100\rangle$ plane. The samples had a 2DEG front gate, 40 and 20 nm (high and low mobility samples, respectively) above the 2DHG and a silicon doped back gate, 300 nm below it[12].

The inset to Fig. 1 depicts a characteristic SdH curve. Two distinct frequencies corresponding to two bands are clearly observed and used to determine the carrier densities in the lighter and heavier bands (p_l and p_h, respectively, not to be confused with the bulk light and heavy bands). Fig. 1 depicts p_l and p_h as a function of the total density, p_{total}, for the high (circles) and low (squares) mobility samples. The band's population in the two samples are similar. Below a total density of about $2\times10^{11}\ \mathrm{cm}^{-2}$ it is hard to resolve two bands in the SdH data. For higher densities, the bands split and for $p_{total} \geq 4\times10^{11}\ \mathrm{cm}^{-2}$ practically all additional carriers populate the heavier, less mobile, band.

The weak field MR of the high mobility sample at $p_{total} = 4.25\times10^{-11}\ \mathrm{cm}^{-2}$, $p_l = 1.52\times10^{-11}\ \mathrm{cm}^{-2}$, $p_h = 2.73\times10^{-11}\ \mathrm{cm}^{-2}$, and different temperatures is presented in the inset to Fig. 2. The Lorentzian shaped PMR expected from two band transport is obtained by subtracting the predicted quantum correction (see below) from the full MR data. The result is depicted in Fig. 2.

The analysis of the high mobility data presented in[12] was based on standard, two-band transport formulae,[28] generalized to include interband scattering.[29,30] The Lorentzian PMR expected for two band transport was extracted by subtracting the weak parabolic negative magnetoresistance (NMR), attributed to Coulomb interactions[40], from the full MR curve. Here we refine the analysis and incorporate quantum corrections *ab initio*. These corrections include hole-hole interaction, WL, and WAL. They all become increasingly important as the sample conductivity is reduced. Their inclusion *ab initio* facilitates a unified analysis of high and low mobility samples. Moreover, the quantum corrections provide valuable information on the fundamental scattering processes in 2DHG.

B. Theoretical background

Our analysis generalizes Choi *et al.*[41] approach to the case of two band transport. The starting point is a 4×4 conductivity matrix for the two bands in the presence of a perpendicular magnetic field. All matrix elements, except the Hall ones, are modified by quantum effects. Setting the Hall currents to zero and inverting the matrix one obtains the longitudinal resistance with WL, WAL, and interaction corrections:

$$\rho_{xx}(H)=\rho_{\scriptscriptstyle L}(H)+f(S_l,S_h,Q,H)\cdot(\delta\sigma_{\scriptscriptstyle WL}+\delta\sigma_{int})\,, \quad (1)$$

where

$$\begin{aligned}\rho_{\scriptscriptstyle L}(H) &= \rho_{\scriptscriptstyle L}(H\to\infty)+\frac{L}{1+(H/W)^2}\,,\\ \rho_{\scriptscriptstyle L}(H\to\infty) &= \frac{R_h^2S_l+R_l^2S_h-2QR_lR_h}{(R_l+R_h)^2}\,,\\ W &= \frac{S_l+S_h+2Q}{R_l+R_h}\,,\\ L &= -\frac{\left[R_l(S_h+Q)-R_h(S_l+Q)\right]^2}{(S_l+S_h+2Q)(R_l+R_h)^2}\,,\end{aligned} \quad (2)$$

and

$$\begin{aligned}\delta\sigma_{\scriptscriptstyle WL} &= \delta\sigma^{ll}_{\scriptscriptstyle WL}+\delta\sigma^{lh}_{\scriptscriptstyle WL}+\delta\sigma^{hl}_{\scriptscriptstyle WL}+\delta\sigma^{hh}_{\scriptscriptstyle WL}\,,\\ \delta\sigma_{int} &= \delta\sigma^{ll}_{int}+\delta\sigma^{lh}_{int}+\delta\sigma^{hl}_{int}+\delta\sigma^{hh}_{int}\,.\end{aligned}$$

Here, l,h correspond to the lighter and heavier heavy hole sub-bands, respectively. $R_i=1/ep_i$, with $i=l,h$, is the Hall coefficient of the i-th band. The diagonal resistances S_l, S_h, and off-diagonal resistance Q can be expressed in terms of elastic and inelastic contributions, $S_l(T)=S_l(0)+\alpha^{-1}[Q(T)-Q(0)]$; $S_h(T)=S_h(0)+\alpha[Q(T)-Q(0)]$, where α is a function of velocities and densities. The resistances $S_l(0)$, $S_h(0)$ pertain to inter and intraband impurity scattering, $Q(0)$ and $Q(T)-Q(0)$ pertain to elastic and inelastic scattering, respectively. The latter processes may include carrier transfer between bands as well as drag-like processes where a particle from one band scatters off a particle in the other band and both carriers maintain their bands. The resistance $\rho_{\scriptscriptstyle L}$ reflects classical, two band PMR and depends in a Lorentzian way on the magnetic field. The conductances, $\delta\sigma_{\scriptscriptstyle WL}$ and $\delta\sigma_{int}$, stand for WL (or WAL) and interaction corrections to the conductivity. The function $f(S_l,S_h,Q,H)$ given in the appendix, is roughly quadratic in H. It is negative for $H<W$ and positive for $H>W$ (see Fig. 25). The functions $\delta\sigma_{\scriptscriptstyle WL}$, $\delta\sigma_{int}$, and $f(S_l,S_h,Q,H)$ depend on both temperature and the magnetic field. Equation (1) shows that the overall quantum contribution to the resistance comprises the corrections to the conductivity of both bands. A qualitative understanding of f can be gained from the single band case where it reduces to $-\rho_0^2\left[1-(\omega_c\tau)^2\right]$, with $\omega_c=eH/mc$ being the cyclotron frequency [cf. Eq. (6)]. The quadratic increase of f with H yields a large interaction correction to the magneto-resistance despite the smallness of $\delta\sigma_{int}$.

We turn now to review the theory for the quantum corrections, WL, WAL, and interaction, taken into account in the data analysis. Further details are provided in Sec. V. We start with WL and WAL. Various authors[34,35,36,37] calculated the hole band structure of asymmetric GaAs/AlGaAs quantum wells and heterostructures and found that each band is characterized by a wave-vector dependent spinor state. When a hole is scattered from $\mathbf{k}$ to $\mathbf{k}'$ the spin-orbit coupling leads to Dyakonov-Perel spin precession around $\mathbf{k}'$ [44,45,46,47,48]. As a result, the spin relaxes at a rate $\hbar/\tau_{so}\approx\epsilon_g^2\tau/\hbar$, where τ is the momentum relaxation time, and ϵ_g is the energy difference between the two bands for an average $k_{\scriptscriptstyle F}$. Since WAL is important for $g\approx1$, where the momentum relaxation rate is similar to the single particle scattering time, we neglect the difference between the two. Scattering between two spin-orbit split bands is hence equivalent to spin-orbit scattering by, e.g., a large atom. For $\tau_{so}<\tau_\varphi$ (τ_φ is the dephasing time), WAL takes place with either positive or negative MR for $l_{\scriptscriptstyle H}=\sqrt{\hbar c/eH}$ larger or smaller than $l_{so}=\sqrt{D\tau_{so}}$ (D is the diffusion coefficient). Averkiev *et al.*[47] calculated the WL correction for weak and strong spin-orbit interaction in symmetric p-type quantum wells. They found that the key parameter for the anomalous MR is $k_{\scriptscriptstyle F}a/\pi$, where a is the well width. This parameter is a measure of bulk heavy/light hole wave function mixing. For $k_{\scriptscriptstyle F}a/\pi\sim1$ they predict PMR at weak fields and NMR at higher fields. Pedersen *et al.*[49] measured such effect in a symmetric GaAs p-type quantum well. In section V B we generalize Averkiev *et al.* procedure to the case of asymmetric GaAs p-type quantum wells with their spin-orbit split bands, taking into account interband and intraband particle-particle propagator contributions to the Cooperon equation. The final result is

$$\begin{aligned}\delta\sigma_{\scriptscriptstyle WL}(H)\equiv\sigma_{\scriptscriptstyle WL}(H)-\sigma_0(H) &= -\frac{e^2}{4\pi^2\hbar} \quad (3)\\ \times\ &\left[2\Psi\left(\frac12+\frac{H_{tr}}{H}\right)-2\Psi\left(\frac12+\frac{\frac12H_{so}+H_\varphi}{H}\right)\right.\\ &\left.-\Psi\left(\frac12+\frac{H_{so}+H_\varphi}{H}\right)+\Psi\left(\frac12+\frac{H_\varphi}{H}\right)\right]\,,\end{aligned}$$

where Ψ is the Digamma function, and the characteristic magnetic fields H_{tr}, H_{so} and H_φ are given by

$$H_{tr}=\frac{\hbar c}{4eD\tau}\,,\qquad H_{so}=\frac{\hbar c}{4eD\tau_{so}}\,,\qquad H_\varphi=\frac{\hbar c}{4eD\tau_\varphi}\,.$$

Using Dyakonov-Perel equation, $\hbar/\tau_{so}\approx\epsilon_g^2\tau/\hbar$, it is then possible to estimate the spin-orbit band splitting, ϵ_g, from transport measurements. The existence of two bands is manifested in three phenomena; a Lorentzian PMR, two SdH frequencies, and finally, WAL correction to the conductivity. While the SdH frequencies merge

into a single frequency when the gap becomes smaller than the scattering rate ($\epsilon_g < \hbar/\tau$), the WAL remains visible down to considerably smaller gaps provided the temperature is low enough. The WAL is hence a powerful tool in the analysis of the 2DHG band structure and scattering mechanisms. The WAL is visible as long as $\tau_{so} \leq \tau_\varphi$. Substituting $\hbar/\tau_\varphi \simeq T/g$ for the dephasing rate we find WAL should be visible as long as $T < g\frac{\hbar}{\tau}\left(\frac{\epsilon_g \tau}{\hbar}\right)^2$, although $\epsilon_g\tau/\hbar$ may be smaller than unity. Moreover, since the relevant magnetic field for WAL is g times smaller than that relevant for the classical effect or the SdH oscillations, the WAL probes the two bands at very small magnetic fields. Winkler *et al.*[37] argue that SdH data at finite fields underestimates the zero field band splitting. Our analysis proposes WAL as a better tool for studying degeneracy lifting of the heavy holes, particularly at weak magnetic fields. The WL correction is significant as long as $l_H \geq l$ or $\sqrt{2}\omega_c\tau g \leq 1$, where $\omega_c = eH/mc$ is the cyclotron frequency and $l = \sqrt{D\tau}$.

We turn now to the interaction corrections[39] to the conductivity. Our analysis follows Choi *et al.*[41] Note the interaction MR is mainly due to the magnetic field dependence of the pre-factor of these corrections, $f(S_l, S_h, Q, H)$ in Eq. (1), rather than the explicit dependence upon H expressed in Eqs. (4) and (5).

The diffuson channel correction is[50,51,52,53]

$$\delta\sigma^D_{int}(T,H) = \qquad (4)$$
$$\begin{cases} -\frac{e^2}{2\pi^2\hbar} g_0 \ln\left(\frac{\hbar}{T\tau}\right) - \frac{e^2\Xi}{4\pi^2\hbar} g_2(h), & \text{for } \frac{\hbar}{T\tau} > 1 \\ \frac{e^2}{2\pi^2\hbar} g_0 \left[\Psi\left(\frac{1}{2}+\frac{\hbar}{T\tau}\right) - \Psi\left(\frac{1}{2}\right)\right] - \frac{e^2\Xi}{4\pi^2\hbar} g_2(h), & \text{for } \frac{\hbar}{T\tau} < 1 \end{cases}$$

where

$$\begin{aligned} g_0 &= 4 - 3\frac{2+F}{F}\ln\left(1+\frac{F}{2}\right), \\ \Xi &= 4\left[\frac{2+F}{F}\right]\ln(1+\frac{F}{2}) - 4, \\ F &= \int_0^{2\pi}\frac{d\theta}{2\pi}\left[1+\frac{2K_F}{\kappa}\sin\left(\frac{\theta}{2}\right)\right]^{-1}, \qquad (5) \\ g_2(h) &= \int_0^\infty d\Omega \frac{d^2}{d\Omega^2}\left[\Omega\nu(\Omega)\right]\ln\left|1-\frac{h^2}{\Omega^2}\right|, \\ h &= g^\star\mu_B H/T, \end{aligned}$$

and

$$g_2(h) = \begin{cases} \ln(h/1.3) & \text{for } h \gg 1, \\ 0.084h^2 & \text{for } h \ll 1. \end{cases}$$

Ψ is the Digamma function, κ is the 2D inverse screening length, $\nu(\Omega)$ is the density of states at an energy $\hbar\Omega$, $g^\star$ is the 2DHG effective g-factor, and μ_B is the Bohr magneton. In the diffuson channel the interaction correction depends on the magnetic field through the Zeeman energy only. The diffusive correction, $\delta\sigma^D_{int}$, is hence independent of H as long as $h \ll 1$. Unlike the cooperon correction that vanishes for $\omega_c\tau > 1/g$, the diffuson correction persists to $\omega_c\tau \simeq 1$.

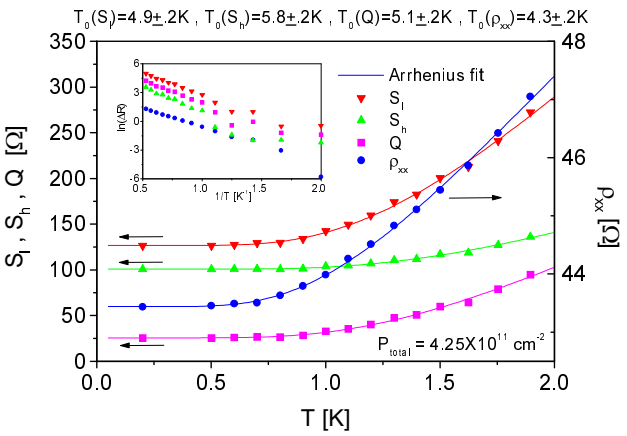

FIG. 3: The various scattering rates expressed as resistances (left axis) and the zero field longitudinal resistance (right axis) vs. T. Solid lines depict best fit to Arrhenius dependence with the characteristic temperatures listed at the top of the figure. Inset - same data in semi log plot.

The cooperon channel correction to the conductivity is given by[54]

$$\begin{aligned} \delta\sigma^C_{int}(T,H) &= -\frac{e^2}{2\pi^2\hbar} g_c(T,H)\ln\left(\frac{T\tau}{\hbar}\right) \\ &\quad -\frac{e^2}{2\pi^2\hbar} g_c(T,H)\phi_2\left(\frac{2eDH}{\pi Tc}\right), \end{aligned}$$

where

$$\begin{aligned} \phi_2(x) &= \int_0^\infty \frac{tdt}{\sinh^2(t)}\left[1-\frac{xt}{\sinh(xt)}\right], \\ \phi_2(x) &= \begin{cases} \ln(x) & \text{for } x \gg 1, \\ 0.30x^2 & \text{for } x \ll 1, \end{cases} \end{aligned}$$

and

$$g_c^{-1}(T,H) = \begin{cases} g_0^{-1} + \ln\left(\frac{1.13E_F}{T}\right) & \text{for } \frac{2eDH}{\pi Tc} < 1, \\ g_0^{-1} + \ln\left(\frac{cE_F}{DeH}\right) & \text{for } \frac{2eDH}{\pi Tc} > 1. \end{cases}$$

The correction depends on H and vanishes for $H > 2\pi H_{tr}$, or equivalently, $\sqrt{2}\omega_c\tau g/2\pi > 1$. The Maki-Thompson correction is ignored.

C. Data analysis

For the high mobility sample, the WL and WAL corrections are negligible above 1 Gauss. The analysis may thus be confined to interband scattering and interaction in the diffuson channel [Eq. (4)[50]]. The full MR is depicted in the inset to Fig. 2. The parabolic background is attributed to Coulomb interaction and analyzed below. Subtracting this background we obtain the data presented in Fig. 2. Fitting these data to Eqs. (2), one

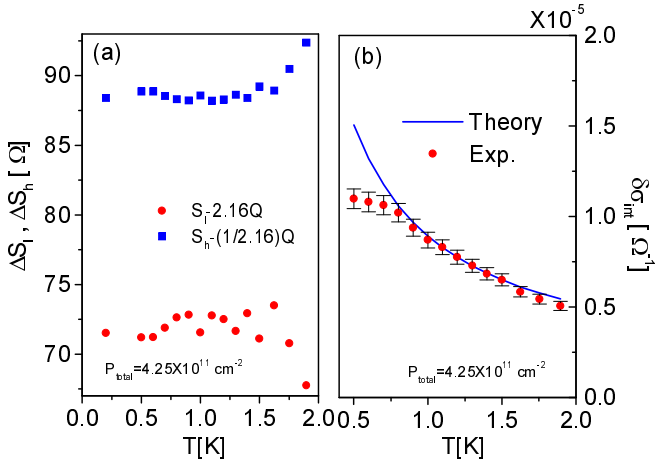

FIG. 4: (a) High mobility sample. $\Delta S_l = S_l - 2.16Q$, $\Delta S_h = S_h - 2.16^{-1}Q$ vs. T for $p = 2 \times 10^{11} cm^{-2}$. (b) Hole-hole interaction correction to the conductance in the diffuson channel, $\delta\sigma^D_{int}$.

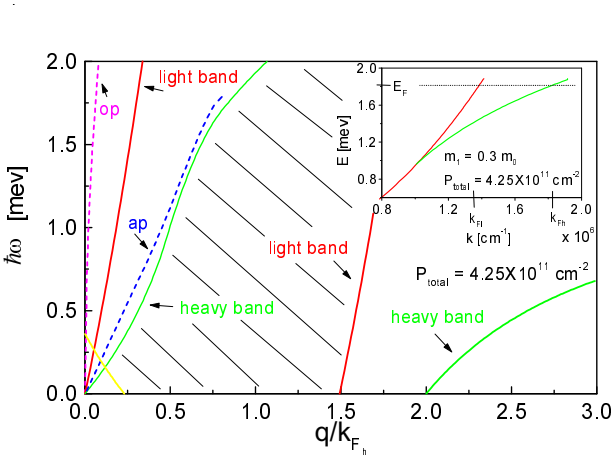

FIG. 5: Solid lines - heavy and light particle-hole excitation continua as a function of momentum scaled to the heavy hole Fermi wave vector. Shaded area corresponds to the range where drag-like interband scattering is possible at very low T. Dashed lines -optical (op) and acoustic (ap) plasmon dispersions. Inset - The measured bands dispersion relations. The energy E_F corresponds to the hole Fermi energy at $p_{total} = 4.25 \times 10^{11}$ cm^{-2}.

obtains $\rho_{xx}(H \to \infty)$, L, and W as a function of temperature and density. Note the excellent agreement with the predicted shape, Eqs. (2). Below $\simeq 0.6$ K, the resistance is practically independent of T while for temperatures above $\simeq 2$ K, the Lorentzian is hardly visible. The suppression of the classical two band magnetoresistance results from interband scattering. At low temperatures this scattering is mainly elastic. As the temperature is increased, inelastic scattering commences, the drift velocities of carriers in the two bands gradually approach each other, and the magnetoresistance is consequently diminished. The extracted functions, S_l, S_h, and Q, together with $\rho_{xx}(H = 0)$, are shown vs. T in Fig. 3 for the same total density as in Fig. 2. At low temperatures, all these quantities saturate to some residual values $S_l(0)$, $S_h(0)$, $Q(0)$ which we attribute to inter and intraband elastic scattering. As the temperature is increased, inelastic scattering commences and these quantities grow.

The remarkable and central result emerging from the high mobility data is the observation that the inelastic scattering rates follow the same temperature dependence as $\rho_{xx}(H = 0)$, namely, $S_i(T) = S_i(0) + \alpha_{S_i} \exp(-T_0/T)$, $Q(T) = Q(0) + \alpha_Q \exp(-T_0/T)$, where α_{S_i}, α_Q are constants. The characteristic temperature, T_0, is similar to all these quantities, including ρ_{xx} (see inset to Fig. 3). For S_l we find $T_0 = 4.9 \pm 0.2$ K, for S_h we find $T_0 = 5.8 \pm 0.2$ K, for Q we find $T_0 = 5.1 \pm 0.1$ K, and for ρ_{xx} we find $T_0 = 4.3 \pm 0.1$ K. We find experimentally [see Fig. 4(a)] that for $T < 1.6$ K, $S_l(T) \simeq S_l(0) + 0.46^{-1}[Q(T) - Q(0)]$; $S_h(T) \simeq S_h(0) + 0.46[Q(T) - Q(0)]$, thus yielding for the density of Figs. 2 and 3, $\alpha = 0.46$. Since the prefactors multiplying Q are reciprocal, the resistances $S_l(0)$ and $S_h(0)$ are identified as the diagonal resistances, pertaining to intraband scattering. The Arrhenius temperature dependence is hence traced to inter-band scattering alone, rendering the intra-band scattering practically temperature independent. We attribute this unexpected scattering rate to the acoustic plasmon mediated Coulomb interaction discussed below. The results are identical to those presented in Ref. 12.

We turn now to analyze the interaction correction to the conductivity. The Coulomb interaction is characterized by F, the angular average of the statically screened Coulomb interaction, given by Eq. (5). With S_l, S_h, Q known from the previous fit, we fit the parabolic background to Eq. (1) to extract $\delta\sigma_{int}$. We find $F = 0.5 \pm .05$ for all T except the lowest ones. This value should be compared with the theoretical value, $F = 0.81$. Fig. 4b compares the experimental $\delta\sigma_{int}$ with the theoretical one as a function of T. For temperatures above 0.8 K, the agreement between theory and experiment is excellent. At lower temperatures the experimental interaction correction is smaller than that predicted by theory. The interaction coefficient, $g_0(F = 0.47)$ [Eq. (5)], is 0.65 ± 0.03, compared with $g_0(F = 0.81) = 0.46$, predicted by theory. It should be noted that the theoretical value is calculated for two identical parabolic bands with $m = 0.3m_0$. The actual band structure is more complex and in fact, non-parabolic. The fact that F is independent of temperature above $0.8K$ supports the attribution of the interaction contribution to the diffuson channel. We emphasize that the saturation of the interaction correction below $0.8K$ is real and does not result from carrier heating. The latter, deduced from the SdH data, proves efficient cooling down to $0.2K$.

In section V we discuss in detail possible reasons for the Arrhenius temperature dependence of S_l, S_h and Q which in turn leads to a similar temperature depen-

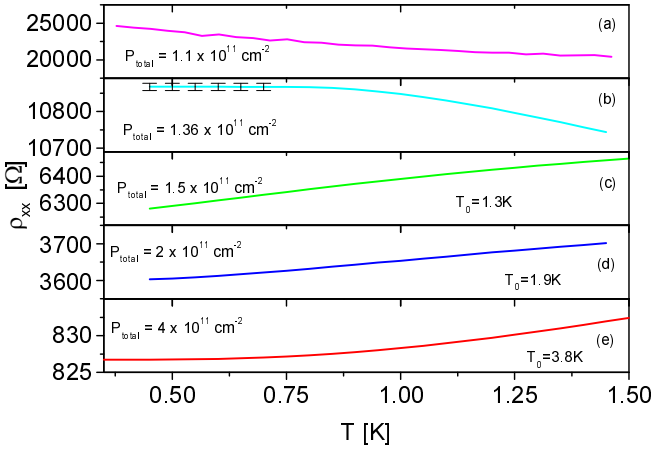

FIG. 6: Low mobility sample. Longitudinal resistance vs. temperature at different carrier densities. In the metallic regime the data are fitted to an Arrhenius function. The characteristic temperature, T_0, is indicated in the figure.

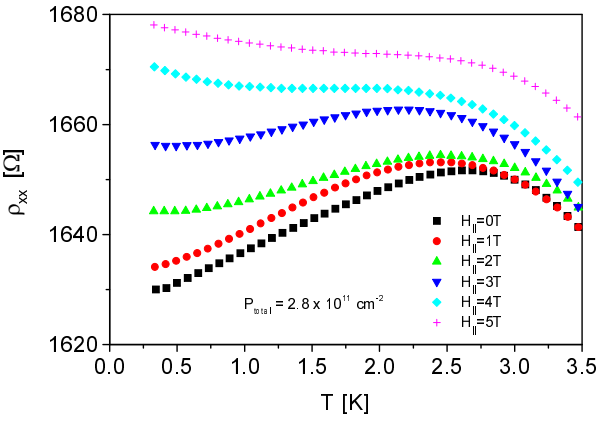

FIG. 7: Low mobility sample. Longitudinal resistance vs. temperature for different parallel magnetic fields. PMR and suppression of the metallic characteristics by the parallel field are evident.

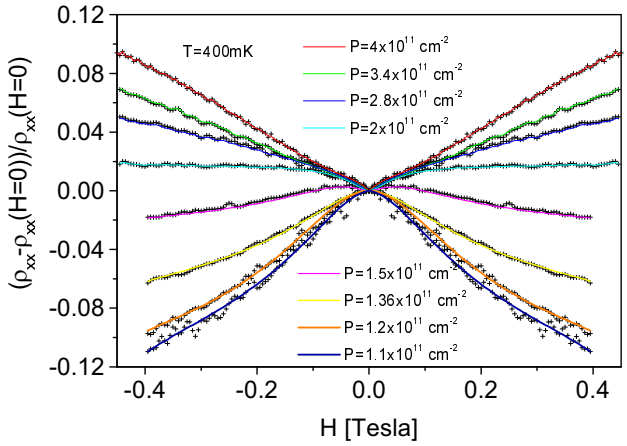

FIG. 8: Low mobility sample. Normalized magnetoresistance at different carrier densities. Data points are marked with crosses while lines correspond to the theory discussed in the text. Note the crossover from PMR to NMR at a density just above the MIT.

dence of ρ_{xx}. These scattering rates (expressed as resistances) crucially depend on the bands' dispersions relations, $E_i(\mathbf{k})$, and their resulting excitation spectra. To extract the bands dispersions depicted in the inset to fig. 5, we approximate[34,35] the light band by a parabolic relation with a mass $m_l = 0.28m_0$ (m_0 is the bare electron mass) which was found from SdH temperature dependence. The variation of p_l, p_h with p_{total}, depicted in fig. 1, is then used to calculate the ratio between the two bands compressibilities. Neglecting band warping as well as differences between density of states and compressibility, we use the ratio of the two compressibilities to extract the dispersion of the heavy band. This dispersion then allows, within the random phase approximation, the calculation of the excitation spectrum of the system. The spectrum is composed of two particle-hole continua, one for each band, and two plasmon branches. Both are shown in fig. 5 for zero temperature.

In summary, we find that the MR of high mobility 2DHG is governed by classical, two band PMR at weak fields and NMR (parabolic background) due to Coulomb interaction in the diffuson channel at stronger fields. The resistance increase with temperature ("metallic phase") follows the inelastic interband scattering. Careful analysis of the interaction contribution to the conductance reveals unexpected saturation of the interaction below $0.8K$.

III. LOW MOBILITY 2DHG SAMPLE

The transition to an insulating behavior in the high mobility sample is taking place at a very low carrier concentration where the sample becomes inhomogeneous. We have therefore preferred to study the transition regime and the insulating phase in a lower mobility sample, $\mu \simeq 20,000$ cm^2/(V s) for $p = 4 \times 10^{11}$ cm^{-2} at 400 mK, where the transition occurs at a moderate density.

Following the high mobility data analysis, we study the magnetoresistance of the low mobility sample and relate it to the temperature dependence of ρ_{xx} at $H = 0$. Since the quantum corrections to the conductivity are order unity in quantum conductance units, the WL, WAL, and interaction correction are more pronounced here compared with the high mobility sample.

In Fig. 8 we present normalized MR measurements at 400 mK for various densities. For high densities, $p \geq 1.5 \times 10^{11}$ cm^{-2}, the weak field MR is positive and $d\rho_{xx}(T, H = 0)/dT > 0$. For 1.5×10^{11} cm^{-2} >

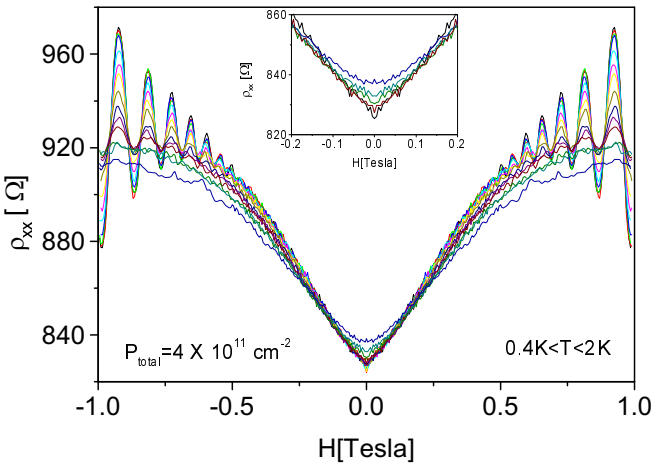

FIG. 9: Low mobility sample. Magnetoresistance curves at different temperatures. Inset - magnified view at $T = 0.4, 0.9, 1.3, 1.5, 2K$. Note the low T, weak field cusp characteristic to WAL.

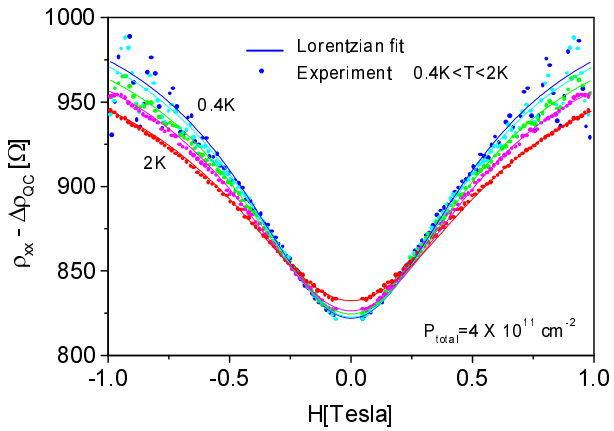

FIG. 10: Low mobility sample. Subtraction of the quantum correction from the longitudinal resistance according to Eq. 1 yields the classical Lorentzian PMR.

$p > p_c = 1.36 \times 10^{11}$ cm^{-2} the MR is negative while $d\rho/dT$ is still metallic. For $p < p_c$ both the MR and $d\rho_{xx}(T, H = 0)/dT$ are negative. From the two SdH frequencies one may extract the carrier densities, p_l and p_h, for the lighter and heavier bands respectively, as depicted in Fig. 1. Below $p_{total} \approx 2 \times 10^{11}$ cm^{-2} the two bands are no longer distinguishable. At higher densities, the expected Lorentzian PMR is found. The MR curves remind Bergmann's data[55] on Mg thin films covered with a fraction of atomic gold layer. In those experiments a crossover from WAL to WL was found as function of the spin-orbit scattering strength tuned by the amount of gold. In our experiment, the role of gold is played by the energy gap between the spin-orbit split bands combined with elastic interband scattering.

We focus first on the high density regime. A set of resistance curves vs. magnetic field, for $p_{total} = 4 \times 10^{-11}$ cm^{-2}, $p_l = 1.7 \times 10^{-11}$ cm^{-2}, $p_h = 2.3 \times 10^{-11}$ cm^{-2} and different temperatures is depicted in Fig. 9. The PMR is dominated by classical MR but near the origin, as evident from the inset to Fig. 9, the experimental points deviate below the Lorentzian curve and form the well known WAL cusp. Eq. (1) contains six independent variables; $\rho_L(H \to \infty)$, L, W, F, τ_φ and τ_{so}. To find them we take advantage of the different magnetic field scales characteristic to WL and WAL compared with the classical MR. Using $H > 10H_{tr} \sim 500$ Gauss data and ignoring WL or WAL corrections we determine 4 parameters, $\rho_L(H \to \infty)$, L, W, and F. We then resort to small magnetic fields and find the remaining two parameters, τ_φ and τ_{so}.

Though the procedure for determining the four parameters is similar to the one used in the high mobility case, the larger quantum corrections lead to uncertainty in F and consequently, in S_h. We have therefore adopted the following strategy. We first fix F to its theoretical value,

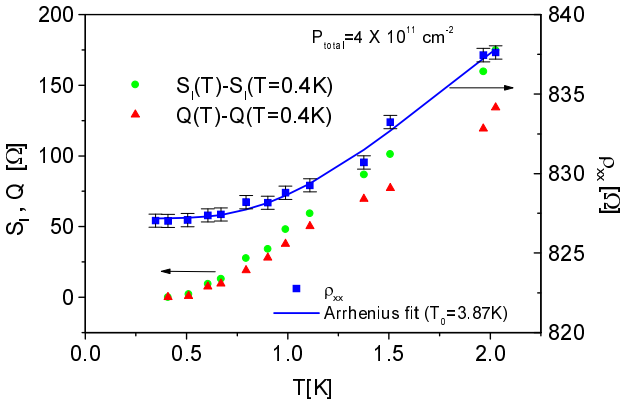

FIG. 11: Low mobility sample. ΔS_l and ΔQ (left axis) and the zero field longitudinal resistance (right axis) vs. T. Solid line depicts best fit to Arrhenius dependence upon temperature.

$F = 0.8$, and calculate $\rho_L(H \to \infty)$, L and W which in turn yield S_l, S_h, and Q. However, the resulting S_h, and Q display a slight nonmonotoneity upon temperature below 0.8 K. Then, for $T < 0.8$ K we tune F to give a monotonous increase of S_l, S_h, and Q with T. The needed change in F is less than 10%. Different values of F, $(F = 1, 0.5)$ give similar results with different S_h. For $F = 1$, the overall change in F is minimal (5%). Fig. 10 depicts the MR data for $F = 1$ after subtraction of the quantum corrections. The agreement with the expected Lorentzian is very good. In Fig. 11, $S_l - S_l(T = 0.4$ K), $Q - Q(T = 0.4$ K), and $\rho_{xx}(H = 0)$ are depicted vs. T for the same total density as in Fig. 9 and $F = 1$. Unlike the high mobility case, the uncertainty in F and hence, S_h, might be substantial. Consequently we limit ourselves to a qualitative comparison between S_l, Q , and

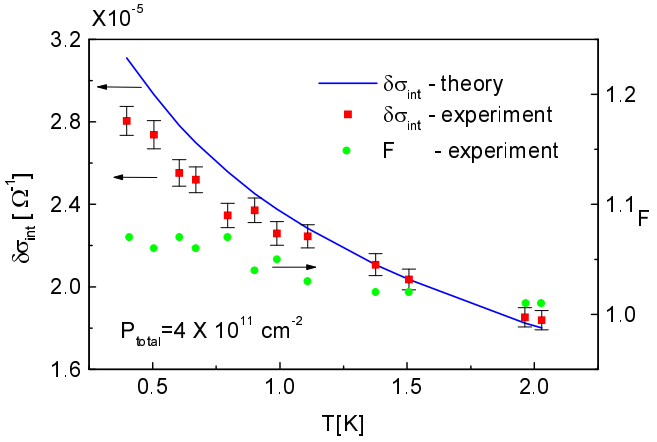

FIG. 12: Low mobility sample. Left axis: Hole-hole interaction correction to the conductivity in the diffuson channel, $\delta\sigma^D_{int}$. Right axis: Angular average of the statically screened Coulomb interaction, F. Theoretical value is $F = 0.9$.

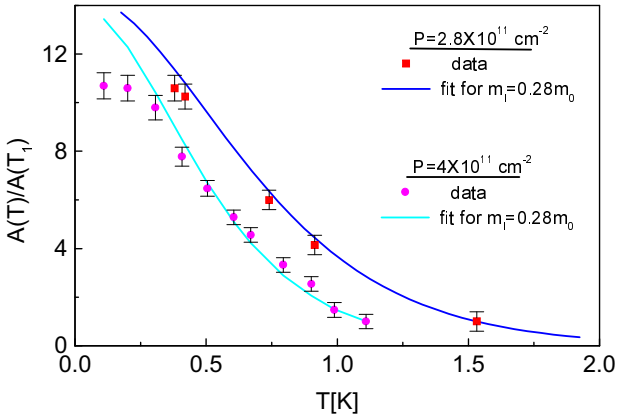

FIG. 13: Shubnikov-de Haas mass analysis. Best fit yields $m_l = 0.28m_0$ where m_0 is the bare electron mass.

$\rho_{xx}(H = 0)$. Examining Fig. 11 one finds a qualitative agreement between the temperature dependence of the three resistances, in agreement with the high mobility data.

Fig. 12 compares the theoretical $\delta\sigma_{int}$ (for $F = 1$), with the measured one as a function of T. For temperatures above 0.8 K, the agreement between theory and experiment is satisfactory, but for temperatures below 0.8 K the interaction correction is again smaller than the predicted value. We emphasize that theory was done for two parabolic bands with $m = 0.3m_0$. The pronounced non-parabolicity of the heavy hole band may affect the interaction contribution significantly. Unlike the high mobility case we do not observe saturation at low temperatures. From the mass analysis of the SdH oscillations, depicted in Fig. 13, one finds $m_l = 0.28m_0$, and no carrier heating above 0.3 K.

Once $\rho_L(H \to \infty)$, L, W, and F are determined one can fit the low magnetic field data to $\sigma(H)-\sigma(H = 0) = \delta\sigma_{WL}(H) + \delta\sigma_{int}(H) - \delta\sigma_{WL}(0) - \delta\sigma_{int}(0)$ and extract τ_φ and τ_{so}. Since the Lorentzian width, W, is larger than H_{tr}, and since the ratio of the thermal and dephasing lengths make the weak field interaction contribution $\sim 5g^2$ times smaller than the WL or WAL one [see Eqs. (3), (4)], the MR for $H \ll H_{tr}$ is dominated by WL or WAL. The uncertainties in F are hence reflected in less than 10% uncertainty in τ_φ and τ_{so}. Fig. 14 presents $\sigma(H) - \sigma(H = 0) - [\sigma_{cl}(H) - \sigma_{cl}(0)]$ for $p_{total} = 2.8 \times 10^{11}$ cm^{-2} where $\sigma_{cl}(H)$ is the classical Drude part of the conductivity. The data agree well with theory, Eq. (3). The resulting τ_φ and τ_{so}, for $p = 2.8\times10^{11}$ cm^{-2} are depicted in Figs. 15 and 16. The error bars reflect the uncertainty in F. The phase breaking rate is linear with temperature, as expected by theory (Fig. 15). The prefactor, however, is five times larger than the theoretical prediction $1/\tau_\varphi = T/(\hbar g)\cdot\ln(g/2)$. These τ_φ values are

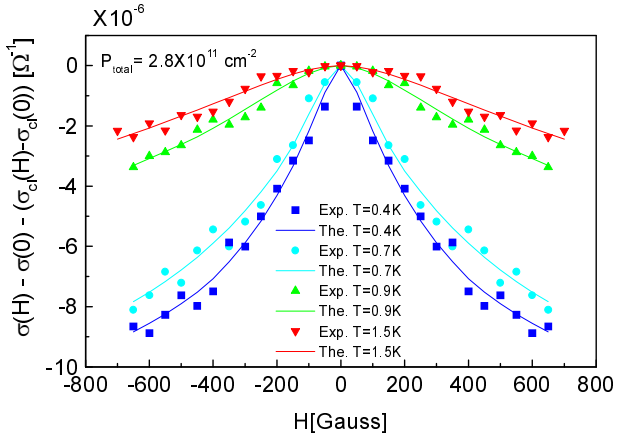

FIG. 14: Low mobility sample. $\sigma(H)-\sigma(0)-(\sigma_{cl}(H)-\sigma_{cl}(0))$ vs. T for $p_{total} = 2.8 \times 10^{11} cm^{-2}$. $\sigma_{cl}(H)$ is the classical Drude conductivity. Theoretical curves correspond to eq. (3). Note the PMR in the whole WAL field range.

consistent with those found in n-type Silicon[56] and p-type GaAs[43] systems. The spin-orbit scattering time, τ_{so}, is as expected practically independent of temperature. The extracted times satisfy $\tau_\varphi > \tau_{so}$ and τ_{so} comparable to τ. Consequently, the WAL PMR should persist in the whole range, $0 < H < H_{tr}$. The band splitting, ϵ_g, may be roughly estimated with the help of the Dyakonov-Perel formula and compared with the value extracted from the dispersion relation (inset to Fig. 5) deduced from SdH oscillations. Close to the MIT the Dyakonov-Perel spin precession depends on the relaxation time, τ, extracted from the decay of the SdH oscillations once the mass has been determined. Fig. 13 depicts the SdH mass analysis for $p = 2.8 \times 10^{11}$ cm^{-2}. The envelope analysis yields $\tau \simeq 10^{-11}$ sec. Substituting τ in Dyakonov-Perel expression one finds $\epsilon_g \simeq 0.5$ mev, which agrees with the

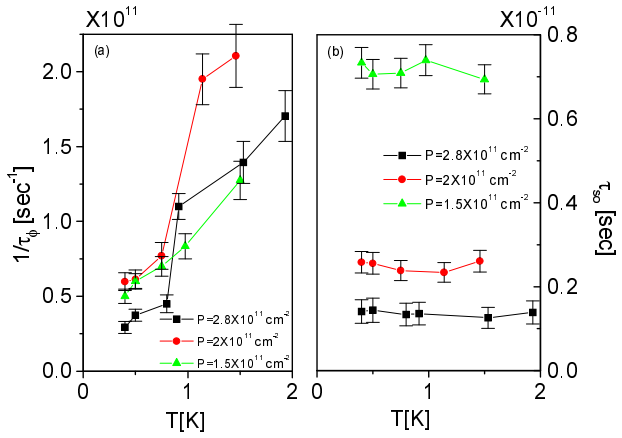

FIG. 15: Low mobility sample. WAL analysis. (a) dephasing rate vs. T at different densities. (b) spin-orbit scattering time vs. T at different densities.

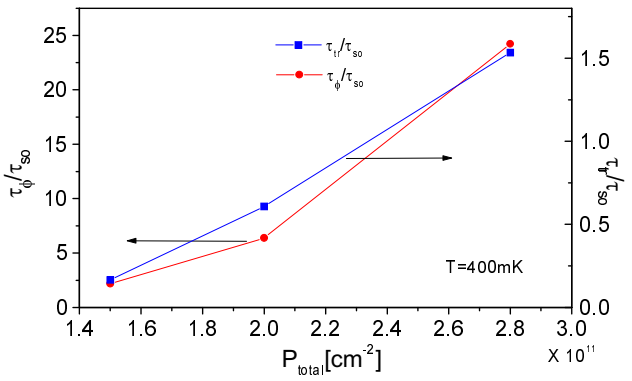

FIG. 16: Low mobility sample. τ_φ/τ_{so} vs. total carrier density (left axis). τ/τ_{so} vs. total carrier density (right axis).

SdH value. This result strongly supports the association of the WAL with scattering between the two spin-orbit split bands and establishes WAL as a powerful tool for measuring ϵ_g.

We turn now to analyze the data corresponding to densities below $p = 2 \times 10^{11}$ cm^{-2} where the Lorentzian classical MR and the two SdH frequencies can not be resolved. Then, Eq. (1) takes the single band form[41],

$$\rho_{xx}(H) = \rho_0 - \rho_0^2 \left[1 - (\omega_c \tau)^2\right] (\delta\sigma_{WL} + \delta\sigma_{int}), \qquad (6)$$

where ρ_0 is the classical longitudinal resistance. There are 4 parameters to be determined, ρ_0, F, τ_φ and τ_{so}. Again, we separate the fitting procedure to $H \gg H_{tr}$ and $H \ll H_{tr}$. Albeit, this time $H_{tr} > 0.1$ T and consequently the WAL or WL corrections are important in the whole magnetic field range, $0 < H < 0.7$ T. The four parameters are found iteratively. In the weak field regime we guess ρ_0 and F and fit $\sigma(H) - \sigma(H = 0)$ to theory with τ_φ and τ_{so} as two fitting parameters. The resulting τ_φ and τ_{so} are plugged into Eq. (6) and the high field data are fitted with ρ_0 and F as two adjustable parameters. This procedure converges after ~ 10 iterations to a self consistent solution. The results of such an analysis for $p = 1.5, 2 \times 10^{11}$ cm^{-2} are presented in Figs. 15 and 16. Again, τ_{so} is practically independent of temperature. Fig. 17 depicts the quantum correction to the magnetoconductivity $\sigma(H) - \sigma(H = 0) - [\sigma_{cl}(H) - \sigma_{cl}(0)]$ for $p_{total} = 2 \times 10^{11}$ cm^{-2}. The data agree well with Eq. (3). Since $H_{so} < H_{tr}$ the MR in Fig. 17 changes sign from positive to negative as the field increases. The weak field PMR results from WAL ($\tau_\varphi > \tau_{so}$) and one may use the Dyakonov-Perel formula to estimate ϵ_g. For $p = 2 \times 10^{11}$ cm^{-2} and $p = 1.5 \times 10^{11}$ cm^{-2} we find $\epsilon_g \simeq 0.3$ mev $\simeq 0.2E_F$ and $\epsilon_g \simeq 0.2$ mev $\simeq 0.16E_F$, respectively. For $p \geq 2.8 \times 10^{11}$ cm^{-2}, the classical PMR as well as the two frequencies of the SdH oscillations are visible implying $\epsilon_g > \hbar/\tau$. For densities below

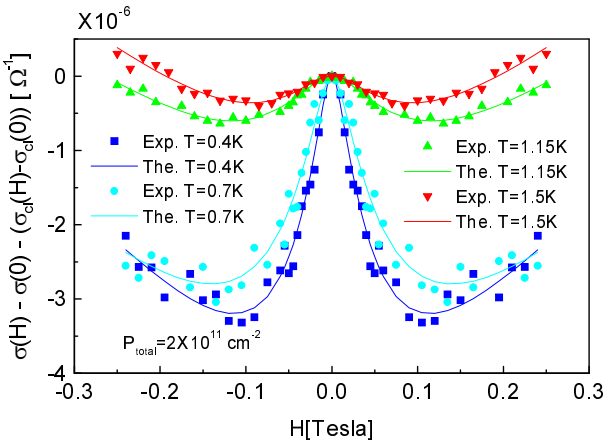

FIG. 17: $\sigma(H) - \sigma(0) - (\sigma_{cl}(H) - \sigma_{cl}(0))$ vs. T for $p_{total} = 2 \times 10^{11}$ cm^{-2}. Theoretical curves correspond to Eq. (3). Note the crossover from PMR to NMR resulting from the fact that $\tau < \tau_{so}$.

2.8×10^{11} cm^{-2}, $\epsilon_g < \hbar/\tau$, and the two bands can be resolved solely by WAL. These results demonstrate that the Lorentzian MR as well as the two SdH frequencies disappear when the band spacing becomes smaller than the level broadening by disorder. The quantum interference, on the other hand, indicates the existence of two bands down to lower densities.

The extracted Coulomb interaction parameter is $F \simeq 1 \pm 0.2$, practically independent of temperature. This value is in good agreement with the theoretical prediction, $F = 0.9$. The resulting ρ_0 increases with temperature. The origin for this temperature dependence is not clear. It might result from inelastic inter-band scattering or other effects such as percolation or temperature dependent screening. Those mechanisms are discussed in the next section.

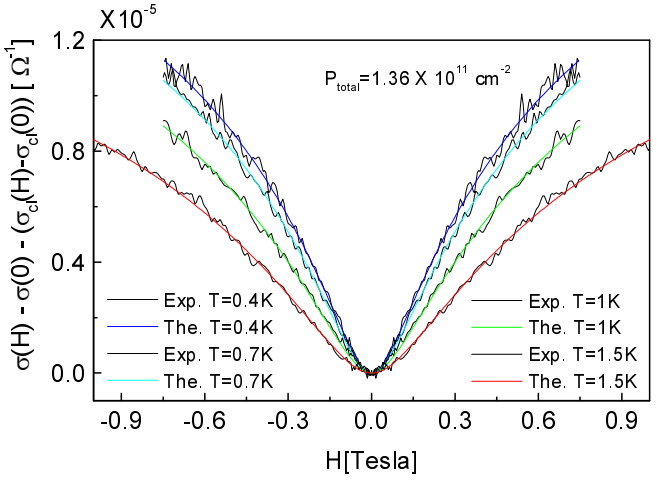

FIG. 18: Low mobility sample. $\sigma(H) - \sigma(0) - [\sigma_{cl}(H) - \sigma_{cl}(0)]$ vs. T for $p_{total} = 1.36 \times 10^{11}$ cm^{-2}. Theoretical curves correspond to the standard WL formula [Eq. (3) with $\tau_{so} \to \infty$].

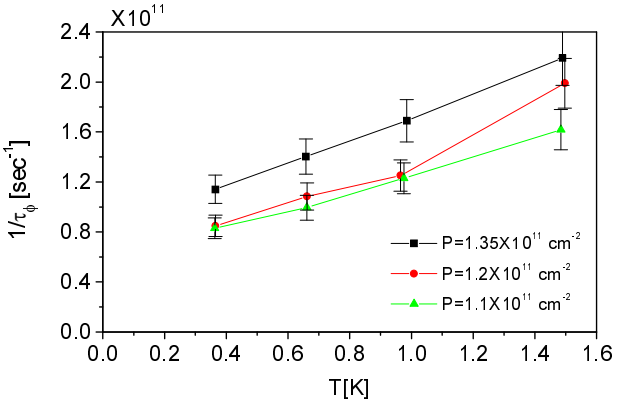

FIG. 19: WL analysis of low mobility sample. Dephasing rate vs. T at different carrier densities. Note the deviation of τ_φ^{-1} from linearity in T as discussed in the text.

For $p \le p_c = 1.36 \times 10^{11}$ cm^{-2}, WL and interaction dominate and lead to NMR. At these densities, $g \le 2.5$, the quantum corrections are on the order of the classical resistance, and the expansion in $1/g$ is only approximate. There are three parameters to be determined: F, τ_φ and τ. Fitting $\sigma(H) - \sigma(H = 0)$ to theory indicates that WL dominates over interaction. Different values of F modify the extracted τ_φ by less than 10%. One may therefore set $F = 1$, and find τ_φ and τ. Fig. 18 depicts the data and a best fit for $p_{total} = 1.35 \times 10^{11}$ cm^{-2}. Fig. 19 displays the extracted dephasing rate for the three lowest densities. Note that $1/\tau_\varphi$ extrapolates to a finite value for $T \to 0$. Similar saturation of τ_φ has been reported by Brunthaler *et al.*[57] in their Si-MOSFET weak localization measurements. We emphasize though that we have used WL theory at the border of its validity, $\delta g \lesssim g$. The extracted τ_φ values might hence be misleading.

IV. DISCUSSION OF DATA ANALYSIS

At high densities, $p > 2 \times 10^{11}$ cm^{-2}, we find that the PMR and temperature dependent resistance are fully consistent with scattering between the two spin-orbit split bands, WAL, and interaction. The resistance increase with temperature is mainly a consequence of inelastic interband scattering. For intermediate densities, 1.36×10^{11} cm^{-2} $< p < 2 \times 10^{11}$ cm^{-2}, WAL indicates two non-degenerate bands. For example, for $p = 2 \times 10^{11}$ cm^{-2} we find $\epsilon_g/E_F \simeq 0.2$, implying roughly 20% difference in densities and resistances of the two bands. For densities smaller than the critical density, $p_c = 1.36 \times 10^{11}$ cm^{-2}, the two bands broadened by disorder merge to form a single band. The classical PMR as well as the WAL vanish and leave a conventional, single band WL NMR. Similar MR is also found in other experiments on p-type GaAs and SiGe[43,58] samples. The zero field WL crosses over to strong localization as the density is further reduced. The MIT we observe reflects in our opinion effective cancellation of the temperature dependence of the resistance due to two competing processes. On one hand the reminiscent band splitting leads to inelastic interband scattering and WAL, both characterized by $d\rho_{xx}/dT > 0$. On the other hand, interaction and WL lead to $d\rho_{xx}/dT < 0$. As the density is reduced, the splitting between the two bands shrinks, their broadening due to disorder is enhanced and they practically merge to form a single, doubly degenerate band. In that process, the effect of inelastic scattering on the resistance is gradually diminished, the WAL turns into WL (τ_φ becomes comparable to τ_{so}), and together with the Coulomb interaction, the sample displays an insulating behavior. The so called MIT is hence just a smooth crossover from two to one band physics. Note that on the metallic side, near the transition, our MR data, as well as other data,[43,58] agree well with WL. Nonetheless, the temperature dependence is opposite to that expected from WL. There should, hence, be some scattering mechanism with opposite T dependence compared with WL and very weak dependence upon magnetic fields. Extrapolating our knowledge from the metallic regime we conjecture that this mechanism is inelastic interband scattering.

In other experiments on higher mobility 2DHG samples[9,10,43], the critical density, p_c, turned out to be lower than that reported here. In Ref. 9, $p_c = 1.25 \times 10^{10}$ cm^{-2}, and in Refs. 10,43, p_c is around 5×10^{10} cm^{-2}. We believe that in those experiments the bands are split down to densities lower than in our experiment, due to the following reasons: (a) For the mobilities of Refs. 9,10, the bands broadening by disorder, and hence the bands mixing, is small. (b) The quantum well asymmetry

and hence the lack of inversion symmetry are more pronounced in those samples. Consequently, the band splitting due to spin-orbit interaction is considerably larger than in our samples even with the lower densities taken into account. The lack of inversion symmetry is particularly pronounced in the p-type inverted semiconductor insulator semiconductor (ISIS) structure[59] used in Ref. 9.

Quantitative estimates of ϵ_g require detailed band structure calculations[36]. Winkler[37] studied band splitting in 2DHG due to lack of inversion symmetry and was able to show that SdH analysis underestimates the difference in carrier partition between the two bands at $H = 0$. For a typical confining potential at $p = 2 \times 10^{10}$ cm^{-2}, Winkler found a 10% difference in hole densities and 20% difference in their masses. The splitting, ϵ_g, turned out to be about 0.5 K. These results confirm the role of two bands in the transport properties of low density 2DHG.

We turn now to discuss some other aspects of the samples that might be relevant for the MIT. Meir[27] pointed out that the 2DHG is probably inhomogeneous near the MIT and analyzed our data in the context of classical percolation. He was able to show that the $H = 0$ low temperature longitudinal resistance can be fitted with $\rho_{xx} = a(p - p^\star)^{-\gamma}$, with $p^\star = 0.9 \pm .05 \times 10^{11}$ and $\gamma = 1.3 \pm 0.1$. For classical percolation, the critical exponent γ should be $4/3 \simeq 1.33$. Identical functional dependence was found for the data of Hanein *et al.*[42] Indications of inhomogeneity are found in thermodynamic measurements as well. Dults and Jiang measured the compressibility, κ, of 2DHG[60], and found that $d\kappa/dp$ changes sign at the critical density. We also measured the same quantity in a different way and found similar results[61]. Si and Varma argue that the inverse compressibility should vanish as the MIT is approached from the metallic side[14]. The argument is that near the transition disorder and Coulomb interaction create inhomogeneous regions (puddles) which behave like weakly coupled quantum dots. The breakdown to puddles leads to Coulomb blockades and incompressibility. Ilani *et al.*[62] used a single electron transistor to measure the local compressibility of a 2DHG and found that below the critical MIT density, the sample is indeed no longer homogenous. At the moment, the importance of inhomogeneity for the MIT is unclear. Inhomogeneity should have an interesting effect on the phase breaking length, l_φ. When puddles are formed, the diffusion within each puddle is much faster than that between puddles. In that case one may imagine a situation where for a limited temperature range l_ϕ seemingly saturates to the puddle size. Fig. 19 depicts $\tau_\phi^{-1} \equiv D/l_\phi^2$ (where l_ϕ is extracted from WL and D is the diffusion constant extracted from the global resistance) as a function of temperature. Indeed τ_ϕ naively extrapolates to a non zero value for $T \to 0$). We do not have though any evidence that links the deviation of τ_ϕ^{-1} from linear T dependence with puddle formation.

Another source of a metallic behavior of 2D systems has been proposed by Gold and Dolgopolov, and Das Sarma and Hwang[24], and was very recently revisited by Zala *et al.*[63] These authors consider impurity screening by the 2DEG. The main dependence of the dielectric function upon temperature results from $2k_F$ back scattering of the electrons. The calculation suggests that $\Delta\sigma/\sigma = f(T/T_F)$ where f is some scaling function. The disorder potential in Si-MOSFET is short ranged and characterized by significant $2k_F$ wave-vector components. In modulation doped semiconductors, however, the separation of the dopant layer from the 2D gas leads to a long range impurity potential with wave vectors considerably smaller than k_F. Nonetheless, Hamilton *et al.*[25] took the function $f(T/T_F)$ as universal function and succeeded to collapse their GaAs hole data (various densities), to a single curve which is linear at small T/T_F, and saturates to a constant value at higher values. We tried a similar analysis but could not find such a universal scaling. Hamilton *et al.*[25] argue that slightly above the critical density, the asymmetry of the confining potential is irrelevant for the resistance change with temperature. By fixing $g = k_F l$, they claim to eliminate the influence of the confining potential shape and conclude that the metallic behavior is due to temperature dependent screening rather than two bands physics. However, in a recent paper, Papadakis *et al.*[19] show that in less symmetric quantum wells, where subband splitting is large, the resistance increase with temperature is large and uncorrelated to the low T resistance. While temperature dependent $2k_F$ screening might be a relevant factor, we find the two band physics essential for understanding our results.

V. THEORETICAL ASPECTS OF 2DHG MAGNETOTRANSPORT

A. Arrhenius temperature dependence of the hole-hole interband scattering rate

1. *Qualitative discussion*

In this section we consider the hole-hole scattering contribution to the resistivity in a two band system. Since the source of band splitting in the system is spin-orbit coupling, two momenta states in different bands generally have overlapping spin wave functions. A finite interband scattering at vanishingly low temperatures (see fig. 3) results from impurity scattering. At higher temperatures, hole-hole scattering commences and due to the different mobilities in the two bands, increases the resistance. Similarly to the $H = 0$ Coulomb drag between two layers, one naively expects a T^2 Coulomb scattering contribution to the resistance. Experimentally we rather find an unexpected Arrhenius dependence upon temperature. Similar T dependence is found in many experiments probing the metallic phase in 2D.

We turn now to analyze the temperature dependence of hole-hole inter-band scattering and show that its enhancement by acoustic plasmons leads to an Arrhenius law for the resistivity at temperatures which are not too

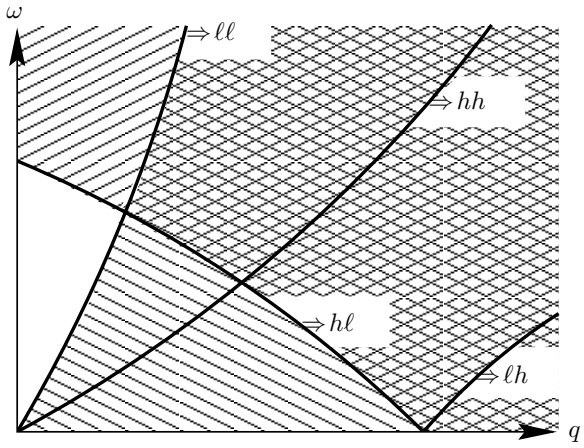

FIG. 20: The (q,ω) plane for small q and ω. The regions in which interband and intraband particle-hole excitations are possible are marked in the figure. The filled regions mark the intraband excitations in the light band ($\ell\ell$) and the interband excitations from the heavy band to the light band ($h\ell$). The scattering process discussed in the text [Eq. (7)] is limited to q and ω in the overlap of both regions.

low.

As discussed in Section V A 2 below, the dominant contribution leading to an Arrhenius T dependence arises from scattering of a light hole off another hole that changes its band in the process (light to heavy or vice versa). The contribution of this process to S_ℓ is given by

$$S_\ell^{(1)} = \frac{1}{4\pi^2}\frac{h}{e^2}\frac{1}{Tp_\ell^2}\int\frac{d^2q}{(2\pi)^2}\int_{-\infty}^{\infty}\frac{\hbar\, d\omega}{\sinh^2(\hbar\omega/2T)} \times |V_{\rm sc}(q,\omega)|^2\,{\rm Im}\chi_{h\ell}^{k_x^2}(\mathbf{q},\omega)\,{\rm Im}\chi_{\ell\ell}(q,\omega)\,, \quad (7)$$

with similar expressions for the contributions to S_h and Q. In Eq. (7), $V_{\rm sc}(\mathbf{q},\omega)$ is the screened Coulomb interaction. The χ functions are response functions generalized to a two band system. They are defined explicitly in Eqs. (12) and (13). Their imaginary parts, appearing in Eq. (7), are non vanishing whenever it is possible to excite a particle-hole pair with momentum $\hbar\mathbf{q}$ and energy $\hbar\omega$ by exciting a particle from band i to band j (with i,j being l,l or h,l).

Fig. 20 depicts regions in the (q,ω) plane for which particle-hole excitations of different types exist (for small q and ω). Intraband excitations are possible only to the right of a line whose slope at the origin corresponds to the Fermi velocity in that band (electron-hole continuum). Interband excitations are forbidden at very small q and ω. At $\omega=0$ the minimal wavevector transfer is $k_F^{(h)}-k_F^{(\ell)}$, while at $q=0$, the minimal energy for excitation from the heavy to the light band corresponds to the band splitting, ϵ_g, between the bands at $k_F^{(\ell)}$. The scattering process described by Eq. (7) is possible at q and ω for which both ${\rm Im}\chi_{\ell\ell}$ and ${\rm Im}\chi_{h\ell}$ are nonvanishing. The various scattering processes are illustrated in fig. 21.

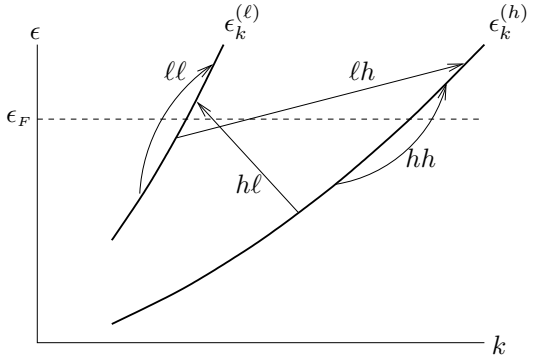

FIG. 21: The arrows represent the different particle-hole excitations. This figure is given for illustration only—the real situation is more complex as momentum space is two-dimensional.

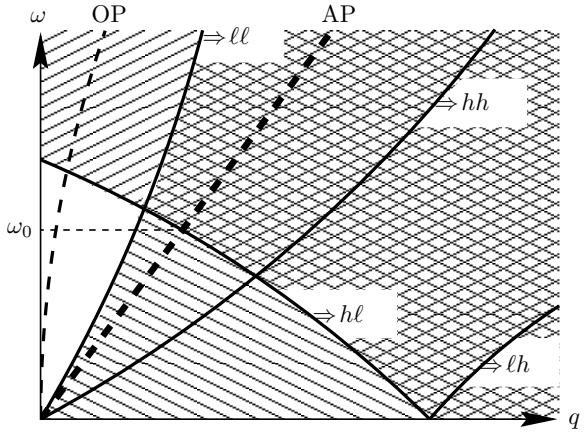

FIG. 22: The (q,ω) plane, for small q and ω. The optical (OP) and acoustic (AP) plasmon branches are shown in dashed lines. The regions in which interband and intraband particle-hole excitations are possible are marked as in fig. 20. The scattering process discussed in the text [eq. (7)] is strongly enhanced along the acoustic plasmon line. As seen in the figure, there is a minimal frequency, ω_0, for this process.

Due to the existence of two bands, the system is characterized by two plasmon branches. The optical branch is essentially governed by the motion of light holes. Its dispersion relation is similar to that of plasmons in a single-band 2D system, namely, $\omega\propto\sqrt{q}$. The acoustic branch is characterized by a linear dispersion, $\omega\propto q$, corresponding to the motion of the heavy holes whose mutual interaction is screened by the light holes. The acoustic mode is hence similar to a sound wave in a metal, namely, ion plasma oscillations screened by electrons. The ions are played here by the heavy holes while the electrons are replaced by light holes. The acoustic plasmon velocity is approximately given by $v_p=\sqrt{m_h/2m_\ell}\,v_F^{(h)}$, certifying, $v_F^{(h)}<v_p<v_F^{(\ell)}$.

The Coulomb scattering depends on the screened

Coulomb potential, $V_{\rm sc}(q,\omega) = V_b(q)/\varepsilon(q,\omega)$, where $\varepsilon(q,\omega)$ is the dielectric function of the system. A large contribution is therefore expected for q and ω close to the plasmon branches where $\varepsilon(q,\omega) = 0$. The Arrhenius temperature dependence of the interband scattering rates results from plasmon enhanced scattering. A similar effect was previously considered for Coulomb drag in double-layer systems[64].

In fig. 22 we plot the (q,ω) plane, this time with the plasmon dispersion lines added. Plasmon enhanced scattering occurs for the process described above *only above a threshold frequency* ω_0. For temperatures $T \ll \hbar\omega_0$, the main contribution comes from frequencies just above the threshold, $\omega_0 < \omega < \omega_0 + T/\hbar$. The contribution of these scattering events is suppressed by a factor $\propto e^{-\hbar\omega/T}$ due to phase space considerations but the plasmon enhancement, compensates for that reduction. The resulting temperature dependence is Arrhenius, $\propto e^{-\hbar\omega_0/T}$.

We turn now to a detailed calculation of the intra and interband scattering rates resulting from plasmon enhanced hole-hole scattering.

2. *Detailed calculations - Boltzmann theory for two bands*

We start by solving Boltzmann equation for the hole-hole interaction contribution to the inter and intraband scattering rates.

For a space and time independent distribution function, $f^{(i)}(\mathbf{k})$ $(i = l, h)$, the Boltzmann equation in the presence of an electric field $\mathbf{E}$ takes the form

$$\frac{e\mathbf{E}}{\hbar}\cdot\frac{\partial f^{(i)}_{\mathbf{k}}}{\partial \mathbf{k}} = \left(\frac{\partial f^{(i)}_{\mathbf{k}}}{\partial t}\right)_{\rm coll}, \tag{8}$$

The collision integral for hole-hole scattering is given by

$$\left(\frac{\partial f^{(i)}_{\mathbf{k_1}}}{\partial t}\right)_{\text{h-h}} = \sum_{ji'j'}\sum_{\mathbf{k_2}\mathbf{k}'_1\mathbf{k}'_2}\left\{-f^{(i)}_{\mathbf{k}_1}f^{(j)}_{\mathbf{k}_2}\left(1-f^{(i')}_{\mathbf{k}'_1}\right)\left(1-f^{(j')}_{\mathbf{k}'_2}\right)W^{ij\to i'j'}_{\mathbf{k}_1\mathbf{k}_2\to\mathbf{k}'_1\mathbf{k}'_2} + f^{(i')}_{\mathbf{k}'_1}f^{(j')}_{\mathbf{k}'_2}\left(1-f^{(i)}_{\mathbf{k}_1}\right)\left(1-f^{(j)}_{\mathbf{k}_2}\right)W^{i'j'\to ij}_{\mathbf{k}'_1\mathbf{k}'_2\to\mathbf{k}_1\mathbf{k}_2}\right\}, \tag{9}$$

where $W^{ij\to i'j'}_{\mathbf{k}_1\mathbf{k}_2\to\mathbf{k}'_1\mathbf{k}'_2}$ is the scattering rate for two holes in states $\mathbf{k}_1$,i and $\mathbf{k}_2$,j to scatter to $\mathbf{k}'_1$,i' and $\mathbf{k}'_2$, j'. Hole-hole scattering satisfies both energy conservation, $W^{ij\to i'j'}_{\mathbf{k}_1\mathbf{k}_2\to\mathbf{k}'_1\mathbf{k}'_2} = w^{ij\to i'j'}_{\mathbf{k}_1\mathbf{k}_2\to\mathbf{k}'_1\mathbf{k}'_2}\,\delta\left(\epsilon^{(i)}_{k_1}+\epsilon^{(j)}_{k_2}-\epsilon^{(i')}_{k'_1}-\epsilon^{(j')}_{k'_2}\right)$, and momentum conservation, $w^{ij\to i'j'}_{\mathbf{k}_1\mathbf{k}_2\to\mathbf{k}'_1\mathbf{k}'_2} \propto \delta_{\mathbf{k}_1+\mathbf{k}_2,\mathbf{k}'_1+\mathbf{k}'_2}$. Using the golden rule we have

$$w^{ij\to i'j'}_{\mathbf{k}_1\mathbf{k}_2\to\mathbf{k}_1-\mathbf{q},\mathbf{k}_2+\mathbf{q}} = \frac{2\pi}{\hbar}|M_{ii'}(\mathbf{k}_1,\mathbf{k}_1-\mathbf{q})|^2\,|M_{jj'}(\mathbf{k}_2,\mathbf{k}_2+\mathbf{q})|^2\,|V_{\rm sc}(q,\omega)|^2\,. \tag{10}$$

Here, $M_{ij}(\mathbf{k},\mathbf{k}')$ are the matrix elements between the spin wavefunctions, derived in Section V C, below.

For convenience we take $\mathbf{v}^{(i)}_{\mathbf{k}} = \hbar\mathbf{k}/m_i$, i.e., neglect non-parabolicity and non-isotropy of the two bands. Linearizing the collision integral for hole-hole scattering, we have

$$\begin{aligned}\left(\frac{\partial f^{(i)}(\mathbf{k}_1)}{\partial t}\right)_{\text{h-h}} = -\frac{1}{4T}\sum_{ji'j'}\sum_{\mathbf{k_2}\mathbf{q}}\int_{-\infty}^{\infty}\frac{\hbar d\omega}{\sinh^2(\hbar\omega/2T)}\,w^{ij\to i'j'}_{\mathbf{k}_1\mathbf{k}_2\to\mathbf{k}_1-\mathbf{q},\mathbf{k}_2+\mathbf{q}}\left(\nu^{(i')}_{\mathbf{k}_1-\mathbf{q}}+\nu^{(j')}_{\mathbf{k}_2+\mathbf{q}}-\nu^{(i)}_{\mathbf{k}_1}-\nu^{(j)}_{\mathbf{k}_2}\right)\\ \times\left[f_0\left(\epsilon^{(i)}_{k_1}\right)-f_0\left(\epsilon^{(i)}_{k_1}-\omega\right)\right]\delta\left(\epsilon^{(i)}_{k_1}-\epsilon^{(i')}_{|\mathbf{k_1}-\mathbf{q}|}-\hbar\omega\right)\left[f_0\left(\epsilon^{(j)}_{k_2}\right)-f_0\left(\epsilon^{(j)}_{k_2}+\omega\right)\right]\delta\left(\epsilon^{(j)}_{k_2}-\epsilon^{(j')}_{|\mathbf{k_2}+\mathbf{q}|}+\hbar\omega\right).\end{aligned} \tag{11}$$

We define the intra and interband response functions,

$$\chi_{ij}(q,\omega) = -\sum_{\mathbf{k}}\frac{f_0\left(\epsilon^{(i)}_{k}\right)-f_0\left(\epsilon^{(j)}_{|\mathbf{k}+\mathbf{q}|}\right)}{\epsilon^{(i)}_{k}-\epsilon^{(j)}_{|\mathbf{k}+\mathbf{q}|}+\hbar\omega+i\delta}|M_{ij}(\mathbf{k},\mathbf{k}+\mathbf{q})|^2\,. \tag{12}$$

In addition, we define response functions with momentum (or current) vertices by adding an appropriate function of $\mathbf{k}$ to the definition

$$\chi^{g(\mathbf{k})}_{ij}(\mathbf{q},\omega) = -\sum_{\mathbf{k}}g(\mathbf{k})\frac{f_0\left(\epsilon^{(i)}_{k}\right)-f_0\left(\epsilon^{(j)}_{|\mathbf{k}+\mathbf{q}|}\right)}{\epsilon^{(i)}_{k}-\epsilon^{(j)}_{|\mathbf{k}+\mathbf{q}|}+\hbar\omega+i\delta}|M_{ij}(\mathbf{k},\mathbf{k}+\mathbf{q})|^2\,. \tag{13}$$

For example, the current-current intraband response function is written in this notation as $\chi^{\mathbf{jj}}_{ii}(\mathbf{q},\omega)$, where $\mathbf{j} = (\mathbf{k}+\mathbf{q}/2)/m_i$. In this example, the function $g(\mathbf{k})$ depends on $\mathbf{q}$ as well.

Solving the linearized Boltzman equation we derive the contribution of hole-hole scattering to the resistivity matrix,

$$\rho_{ik}^{\text{h-h}} = \frac{1}{4\pi^2}\frac{h}{e^2}\frac{1}{Tp_ip_k}\sum_{ji'j'}\sum_{\mathbf{q}}\int_{-\infty}^{\infty}\frac{\hbar d\omega}{\sinh^2(\hbar\omega/2T)}|V_{\text{sc}}(q,\omega)|^2 \tag{14}$$
$$\times\Big\{\text{Im}\chi_{ii'}^{k_x(k_x+q_x)}(-\mathbf{q},-\omega)\text{Im}\chi_{jj'}(\mathbf{q},\omega)\delta_{i'k}+\text{Im}\chi_{ii'}^{k_x}(-\mathbf{q},-\omega)\text{Im}\chi_{jj'}^{k_x+q_x}(\mathbf{q},\omega)\delta_{j'k}$$
$$-\text{Im}\chi_{ii'}^{k_x^2}(-\mathbf{q},-\omega)\text{Im}\chi_{jj'}(\mathbf{q},\omega)\delta_{ik}-\text{Im}\chi_{ii'}^{k_x}(-\mathbf{q},-\omega)\text{Im}\chi_{jj'}^{k_x}(\mathbf{q},\omega)\delta_{jk}\Big\}\,.$$

The dominant contribution to Eq. (14) is given by Eq. (7). In this process a hole changes its band by scattering off a hole in the light band ($i=j=j'=\ell$, $i'=h$ or $i=i'=j'=\ell$, $j=h$ or $i=i'=j=\ell$, $j'=h$). Other contributions are readily extracted from Eq. (14). For example, for the $\ell\ell$ component of the resistivity matrix there are four additional contributions:

- Interband Coulomb drag ($i=i'=\ell$, $j=j'=h$). This is the only term remaining in cases of vanishing matrix elements between the spin wavefunctions of the two bands, e.g., in the absence of spin-orbit coupling:

$$\rho_{\ell\ell}^{D} = \frac{1}{8\pi^2}\frac{h}{e^2}\frac{1}{Tp_\ell^2}\int\frac{d^2q}{(2\pi)^2}\int_0^\infty\frac{\hbar\,d\omega}{\sinh^2(\hbar\omega/2T)} \tag{15}$$
$$\times\,q^2\,|V_{\text{sc}}(q,\omega)|^2\,\text{Im}\chi_{\ell\ell}(q,\omega)\,\text{Im}\chi_{hh}(q,\omega)\,.$$

- Band exchange ($i=j'=\ell$, $i'=j=h$):

$$\rho_{\ell\ell}^{(2)}=\frac{1}{4\pi^2}\frac{h}{e^2}\frac{1}{Tp_\ell^2}\int\frac{d^2q}{(2\pi)^2}\int_{-\infty}^{\infty}\frac{\hbar\,d\omega}{\sinh^2(\hbar\omega/2T)}|V_{\text{sc}}(q,\omega)|^2$$
$$\times\left\{\text{Im}\chi_{h\ell}^{k_x^2}(\mathbf{q},\omega)\text{Im}\chi_{h\ell}(q,\omega)-\left[\text{Im}\chi_{h\ell}^{k_x}(\mathbf{q},\omega)\right]^2\right\}. \tag{16}$$

- Two holes scatter from one band to the other ($i=j=\ell$, $i'=j'=h$):

$$\rho_{\ell\ell}^{(3)}=\frac{1}{4\pi^2}\frac{h}{e^2}\frac{1}{Tp_\ell^2}\int\frac{d^2q}{(2\pi)^2}\int_{-\infty}^{\infty}\frac{\hbar\,d\omega}{\sinh^2(\hbar\omega/2T)}|V_{\text{sc}}(q,\omega)|^2$$
$$\times\Big\{\text{Im}\chi_{\ell h}^{k_x^2}(\mathbf{q},\omega)\text{Im}\chi_{h\ell}(q,\omega)+\text{Im}\chi_{\ell h}^{k_x}(\mathbf{q},\omega)\text{Im}\chi_{h\ell}^{k_x+q_x}(\mathbf{q},\omega)\Big\}. \tag{17}$$

- One particle changes its band by scattering off a heavy hole ($i=\ell$, $j=i'=j'=h$):

$$\rho_{\ell\ell}^{(4)} = \frac{1}{4\pi^2}\frac{h}{e^2}\frac{1}{Tp_\ell^2}\int\frac{d^2q}{(2\pi)^2}\int_{-\infty}^{\infty}\frac{\hbar\,d\omega}{\sinh^2(\hbar\omega/2T)} \tag{18}$$
$$\times\,|V_{\text{sc}}(q,\omega)|^2\,\text{Im}\chi_{\ell h}^{k_x^2}(\mathbf{q},\omega)\,\text{Im}\chi_{hh}(q,\omega)\,.$$

The analogous expression for ρ_{hh} is derived directly from ρ_{ll} by interchanging band indices, $\ell\leftrightarrow h$. Using momentum conservation, we find that the general structure of the hole-hole scattering contribution to the resistivity is given by

$$\rho^{\text{h-h}}\propto\begin{pmatrix}\frac{1}{n_\ell^2} & -\frac{1}{n_\ell n_h}\\ -\frac{1}{n_\ell n_h} & \frac{1}{n_h^2}\end{pmatrix}. \tag{19}$$

The latter matrix has a zero determinant and hence, in the absence of other scattering, allows for dissipationless flow of current of equal velocity in the two bands.

We now focus on the dominant contribution, Eq. (7). We begin with the calculation of the screened Coulomb interaction. The interaction and the response functions are described by 2×2 matrices, with indices corresponding to the two bands. Within the random phase approximation

$$\hat{V}_{\text{sc}}=\hat{V}_{\text{bare}}\left(1+\hat{\chi}\hat{V}_{\text{bare}}\right)^{-1}, \tag{20}$$

where

$$\hat{V}_{\text{bare}}=\begin{pmatrix}V_b & V_b\\ V_b & V_b\end{pmatrix},\quad \hat{\chi}=\begin{pmatrix}\chi_{\ell\ell} & \chi_{\ell h}\\ \chi_{h\ell} & \chi_{hh}\end{pmatrix}. \tag{21}$$

It follows from these equations that all screened interaction matrix elements are identical and given by $V_{\text{sc}}(q,\omega)=V_b(q)/\varepsilon(q,\omega)$, where $V_b(q)=2\pi e^2/\epsilon q$ is the bare interaction (ϵ is the dielectric constant of the host material). The dielectric function is given by

$$\varepsilon(q,\omega)= \tag{22}$$
$$1+\left[\chi_{\ell\ell}(q,\omega)+\chi_{\ell h}(q,\omega)+\chi_{h\ell}(q,\omega)+\chi_{hh}(q,\omega)\right]V(q)\,.$$

Plasmon excitations occur at wavevectors and frequencies which satisfy $\varepsilon[q,\omega_p(q)-i\gamma_p(q)]=0$, where $\omega_p(q)$ is the plasmon frequency and $\gamma_p(q)$ its width. To a good approximation, spin overlap may be ignored in the calculation of plasmons. Within this approximation, the intraband response functions are given by

$$\chi_{ii}(q,\omega)= \tag{23}$$
$$\begin{cases}\dfrac{m_i}{2\pi\hbar^2}\left\{1+i\left[\left(qv_F^{(i)}/\omega\right)^2-1\right]^{-1/2}\right\} & \text{for } \omega<qv_F^{(i)}\\[2ex] \dfrac{m_i}{2\pi\hbar^2}\left\{1-\left[1-\left(qv_F^{(i)}/\omega\right)^2\right]^{-1/2}\right\} & \text{for } \omega>qv_F^{(i)}\,.\end{cases}$$

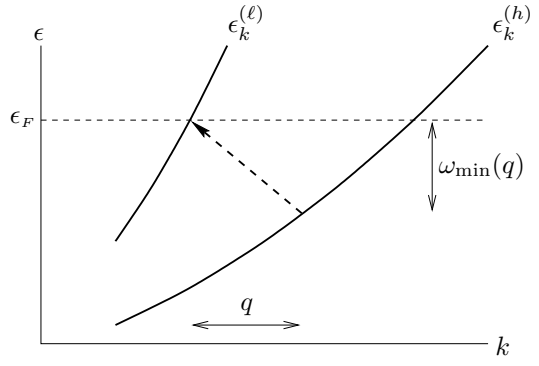

FIG. 23: Dashed arrow represents particle-hole excitation from the heavy to the light band at the minimal energy $\omega_{min}(q)$ for a given momentum q (for $q < k_F^{(h)} - k_F^{(\ell)}$). This transition corresponds to excitation of a heavy hole at $k_F^{(\ell)} + q$ to the light band at $k_F^{(\ell)}$ in exactly the same direction in momentum space.

There are two plasmon branches in the system. The optical branch, with $\omega \propto \sqrt{q}$, results from the solution of $\varepsilon(q,\omega) = 0$ with $\omega > q v_F^{(i)}$ in both bands. The acoustic branch $\omega \propto q$ appears at frequencies, $\omega < q v_F^{(\ell)}$.

Solving for the acoustic branch, we find to lowest order in $\sqrt{m_\ell/m_h}$ that $\varepsilon(q,\omega) = 0$ for $\omega(q) = v_p q - i\gamma q$, where

$$v_p - i\gamma = \sqrt{\frac{m_h}{2m_\ell}} v_F^{(h)} - i \frac{k_F^{(h)}}{4k_F^{(\ell)}} v_F^{(h)} \tag{24}$$

The screened interaction in the vicinity of the plasmon frequency is given by

$$V_{\rm sc}(q,\omega) = V_p \frac{\gamma q}{\omega - v_p q + i\gamma q}\,. \tag{25}$$

Here, V_p is the interaction strength at the plasmon peak. Expanding the denominator to second order in $\sqrt{m_\ell/m_h}$, we find

$$V_p = \frac{2\pi\hbar^2}{m_\ell} \frac{v_F^{(\ell)}}{v_F^{(h)}} \left(\sqrt{\frac{m_h}{2m_\ell}} + i \frac{k_F^{(h)}}{k_F^{(\ell)}} \right)^{-1}\,. \tag{26}$$

In the equations above we have used $\sqrt{m_\ell/m_h}$ as a small parameter. At low densities this approximation breaks down but the plasmon dispersion remains linear and the interaction can still be approximated in the vicinity of the plasmon pole by eq. (25) with slightly different values of v_p, γ, and V_p. The integral over frequency in (7) is approximated in the vicinity of the plasmon frequency using

$$|V_{\rm sc}(q,\omega)|^2 = \pi\gamma q |V_p|^2 \delta(\omega - v_p q)\,. \tag{27}$$

We turn now to the calculation of the interband response function. An interband particle-hole excitation from the heavy to the light band at wavevector $\mathbf{q}$ and frequency ω may occur at wavevectors $\mathbf{k}$ satisfying $\hbar\omega = \epsilon_k^{(\ell)} - \epsilon_{|\mathbf{k}-\mathbf{q}|}^{(h)}$. Possible $\mathbf{k}$ values are dictated by the δ function in the expression for ${\rm Im}\chi_{h\ell}$,

$$\begin{aligned} {\rm Im}\chi_{{\rm h}\ell}^{{\rm k_x^2}}({\rm q},\omega) = \pi \sum_{\rm k} ({\rm k_x} - {\rm q_x})^2 |{\rm M_{h\ell}}(\mathbf{k}-\mathbf{q},\mathbf{k})|^2 \\ \times \left[f_0\left(\epsilon_{|\mathbf{k}-\mathbf{q}|}^{(h)}\right) - f_0\left(\epsilon_k^{(\ell)}\right) \right] \delta\left(\epsilon_{|\mathbf{k}-\mathbf{q}|}^{(h)} - \epsilon_k^{(\ell)} + \hbar\omega\right). \end{aligned} \tag{28}$$

The possible phase space for interband particle-hole excitations is limited by a minimal frequency, $\omega_{\min}(q)$. This frequency is illustrated in fig. 20 as the threshold for particle-hole excitation from the heavy to the light band. Such excitation is realized when the initial heavy hole momentum, $\mathbf{k} - \mathbf{q}$, and the final light hole momentum, $\mathbf{k}$, are parallel and the final energy in the light band is equal to the Fermi energy (fig. 23). The angle, θ, between $\mathbf{k}$ and $\mathbf{q}$ for such an excitation is π. We are interested in excitations with frequencies close to $\omega_{\min}(q)$. Therefore, the angle θ is close to π, and $\lambda = 1 + \cos\theta$ is a small parameter.

Using (57), the interband spinor overlap appearing in (28) is given to leading order in λ (and approximating $k = k_F^{(\ell)}$) by

$$|M_{h\ell}(\mathbf{k}-\mathbf{q},\mathbf{k})|^2 = \frac{9}{2}\mathcal{C}_1 \frac{q^2}{\left(k_F^{(\ell)} + q\right)^2} \lambda\,, \tag{29}$$

where $\mathcal{C}_1 = \left(\langle \xi_H^{(h)} | \xi_H^{(\ell)} \rangle + 1/3 \langle \xi_L^{(h)} | \xi_L^{(\ell)} \rangle \right)^2$ measures heavy/light hole mixing and its magnitude is approximately 1 (exactly 1 in the absence of mixing). The integrals in (28) may now be calculated to leading order in λ (using $d\theta = d\lambda/\sqrt{2\lambda}$) to yield

$$\begin{aligned} {\rm Im}\chi_{h\ell}(q,\omega) &= \frac{3\,\mathcal{C}_1}{2\sqrt{2}\,\pi} \frac{k_F^{(\ell)} q^2}{\hbar^2 \left(k_F^{(\ell)} + q\right)^2 \Delta v(q)} \lambda_{\rm max}^{3/2} \qquad (30) \\ \Delta v(q) &= v_F^{(\ell)} - v_{k_F^{(\ell)}+q}^{(h)}\,, \qquad (31) \end{aligned}$$

and

$$\lambda_{\rm max} = \frac{m_h}{\hbar k_F^{(\ell)} q} \left[\omega - \omega_{\min}(q)\right]. \tag{32}$$

$\lambda_{\rm max}$ represents the maximal deviation of the particle-hole excitation from $\theta = \pi$ with $k = k_F^{\ell}$. Note that ${\rm Im}\chi_{h\ell}(q,\omega) \propto [\omega - \omega_{\min}(q)]^{3/2}$. For the calculation of the resistivity $\rho_{ij}^{(1)}$ we need ${\rm Im}\chi_{h\ell}^{k_x^2}$, eq. (28). Since the main contribution comes from a small range of $\mathbf{k}$ around $-k_F^{(\ell)}\hat{\mathbf{q}}$, we readily obtain

$${\rm Im}\chi_{h\ell}^{k_x^2}(\mathbf{q},\omega) = \left(k_F^{(\ell)} + q\right)^2 \cos^2\varphi\, {\rm Im}\chi_{h\ell}(q,\omega)\,, \tag{33}$$

where φ is the angle between $\mathbf{q}$ and $\hat{\mathbf{x}}$.

We now have all the ingredients needed for evaluating S_l, Eq. (7). The interaction term, $|V_{\rm sc}|^2$, is given

by Eq. (27), so that all terms are calculated along the acoustic plasmon dispersion line, $\omega = v_p q$. The interband response function $\mathrm{Im}\chi_{h\ell}^{k_x^2}$ is given by Eqs. (30)–(33), limiting the integration range to $q > q_0$ (or $\omega > \omega_0 = v_p q_0$). The intraband response of the light holes is given by

$$\mathrm{Im}\chi_{\ell\ell}(q,\omega) = \frac{m_\ell}{2\pi\hbar^2}\frac{\omega}{q v_F^{(\ell)}}\frac{|M_{\ell\ell}|^2}{\sqrt{1-\left(\omega/q v_F^{(\ell)}\right)^2}}\,. \qquad (34)$$

Here, $|M_{\ell\ell}|^2 = |M_{\ell\ell}(\mathbf{k},\mathbf{k}+\mathbf{q})|^2$ (57), calculated at a wavevector $\mathbf{k}$ contributing to $\mathrm{Im}\chi_{\ell\ell}(q,\omega)$ (since $\hbar\omega \ll E_F$, the matrix elements are approximately the same). The integral (7) is calculated assuming $T < \hbar\omega_0$, hence, $\sinh^{-2}(\hbar\omega/2T) \approx e^{-\hbar\omega/T}/4$. The integral is thus limited to the vicinity of $q = q_0$ and $\omega = \omega_0$. The temperature dependence of $S_l^{(1)}$ is readily evaluated,

$$\begin{aligned} S_l^{(1)} &\propto \frac{1}{T}e^{-\hbar\omega_0/T}\int_{q_0}^{\infty} dq\,(q-q_0)^{3/2}e^{-\hbar v_p(q-q_0)/T} \\ &\propto T^{3/2}e^{-\hbar\omega_0/T}\,. \end{aligned} \qquad (35)$$

We thus find that as a result of the minimal frequency for interband excitations, $\rho_{ij}^{(1)}$ displays Arrhenius dependence upon T with a characteristic energy $T_0 = \hbar\omega_0$. The magnitude and the $T^{3/2}$-dependence of the prefactor are determined by details in the vicinity of the threshold for excitations. Collecting all terms and converting the scattering rate into resistivity one obtains

$$\begin{aligned} \rho_{ij}^{(1)} &= (-1)^{\delta_{ij}}\frac{9\sqrt{\pi}}{8}\mathcal{C} \qquad (36) \\ &\times \frac{h}{e^2}\frac{n_\ell^2}{n_i n_j}\left(\frac{m_h}{m_\ell}\right)^{3/2}\left(\frac{q_0}{k_F^{(\ell)}}\right)^{5/2}\left(\frac{T}{E_F}\right)^{3/2}e^{-\hbar\omega_0/T}\,. \end{aligned}$$

The term $\mathcal{C}$ is given by

$$\begin{aligned} \mathcal{C}^{-1} &= \frac{1}{\mathcal{C}_1|M_{\ell\ell}|^2} \qquad (37) \\ &\times \left|1+i\sqrt{\frac{2m_\ell}{m_h}}\frac{k_F^{(h)}}{k_F^{(\ell)}}\right|^2\left(1-\frac{v_{k_F^{(\ell)}+q_0}^{(h)}}{v_F^{(\ell)}}\right)\sqrt{1-\left(\frac{v_p}{v_F^{(\ell)}}\right)^2}\,. \end{aligned}$$

We have considered here the plasmon enhanced contribution to one of the scattering processes described in Section V A 2. With the help of Fig. 22 we note that the only other plasmon enhanced scattering process involves carrier exchange between bands as described by $\rho_{ij}^{(2)}$, Eq. (16). The latter contribution comprises, however, two terms that cancel each other within our approximation for the interband response function. Another possibility involving thermal activation of $\mathrm{Im}\chi_{ij}$ beyond its zero temperature boundaries, in the Coulomb drag term, is discussed in Ref. 12. Thermal activation of plasmons leads to an Arrhenius dependence as well but with a $T^{7/2}$ prefactor.[65] That contribution is hence smaller at low temperatures. A full quantitative calculation takes all contributions into account.

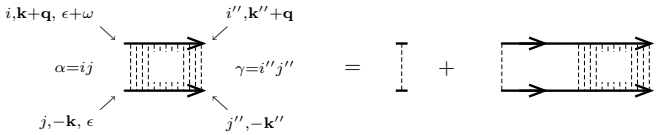

FIG. 24: Diagram for the Cooperon (see Eq. 38) The dashed line describes the short-range disorder.

A T^2 contribution to the resistivity should arise from the different scattering processes at frequencies $\omega < T$. Preliminary calculations indicate this term should be observable in the experiment. Its absence is hence surprising. This discrepancy between theory and experiment might be related to one or more of the approximations involved in the calculation. These include the use of response functions calculated for $q \ll k_F$ at large wavevectors, $q \approx 2k_F$, and the neglect of the anisotropy and nonparabolicity of the heavy band.

B. Quantum interference corrections

In this section we discuss quantum interference corrections to the conductivity. We assume a short-range interaction and take the overlap between spin wavefunctions of the two bands, Eq. (57) into account. We find that in the limit of a small interband gap, the physics is similar to that of electrons in the presence of spin-orbit interaction. Quantum interference corrections in this case were previously studied theoretically in refs.[46,47,66,67,68]. Having calculated the Cooperon, the usual derivation (see, e.g, ref.[66]) is followed to obtain the correction to the conductivity.

The following notation is used: Band indices of one particle are marked by Roman letter $(i, j, \ldots)$ that take the value ℓ or h. Greek letters $(\alpha, \beta, \ldots)$ denote band indices of the Cooperon two particles, taking the values $\ell\ell$, ℓh, $h\ell$ or hh. In this notation, the Cooperon is a 4×4 matrix with Greek indices describing the bands of the incoming and outgoing particles. The Cooperon is given diagrammatically in fig. 24. At a total momentum $\mathbf{q} = 0$ and a total energy $\omega = 0$ it is given by (in this section we use units in which $\hbar = 1$)

$$\begin{aligned} C_{\alpha\gamma}(\mathbf{k},\mathbf{k}'') &= \mathcal{V}_{\alpha\gamma}(\mathbf{k},\mathbf{k}'') \qquad (38) \\ &+ \sum_\beta \int \frac{d^2k'}{(2\pi)^2}\mathcal{V}_{\alpha\beta}(\mathbf{k},\mathbf{k}')G_{i'}^{+}(\mathbf{k},\epsilon)G_{j'}^{-}(-\mathbf{k},\epsilon)C_{\beta\gamma}(\mathbf{k}',\mathbf{k}''), \end{aligned}$$

The Green function is given by

$$G_j^{\pm}(\mathbf{k},\epsilon) = \frac{1}{\epsilon - \epsilon_{\mathbf{k}}^{(j)} \pm i/2\tau_j}\,, \qquad (39)$$

where τ_j is the mean free time in the j^{th} band, calculated from the disorder within the Born approximation. The

Green functions in Eq. (38) limit the contributing momenta to the vicinity of the Fermi surface. Taking the momenta on the Fermi surface, the integration over the magnitude $\mathbf{k}'$ is performed to give

$$C_{\alpha\gamma}(\theta,\theta'') = \mathcal{V}_{\alpha\gamma}(\theta,\theta'') + \sum_\beta \int \frac{d\theta'}{2\pi} \mathcal{V}_{\alpha\beta}(\theta,\theta')\Pi_\beta C_{\beta\gamma}(\theta',\theta''). \tag{40}$$

with

$$\Pi_{\alpha=ij} = \int \frac{d^2k}{(2\pi)^2} G_i^{(+)}(\mathbf{k},\epsilon) G_j^{(-)}(-\mathbf{k},\epsilon)\,, \tag{41}$$

Finally, the disorder line is given by

$$\mathcal{V}_{\alpha=ij,\beta=i'j'}(\theta,\theta') = \left\langle V^2 \right\rangle M_{ii'}(\Delta\theta) M_{jj'}(\Delta\theta)\,. \tag{42}$$

with $\left\langle V^2 \right\rangle$ being the disorder correlation function. Note the overlap between spin wavefunctions (57) is taken here on the Fermi surface and therefore depends on the angle difference $\Delta\theta = \theta' - \theta$ only.

We discuss below two limits; A large band gap, $\epsilon_g\tau \gg 1$, as expected at high densities, and a small band gap, $\epsilon_g\tau \ll 1$, which becomes relevant as the density approaches the metal-insulator transition. In both cases, for a short range disorder, the Cooperon equation can be solved exactly by calculating $C = (1 - \mathcal{V}\Pi)^{-1}\mathcal{V}$.

We start with the high density limit, $\epsilon_g\tau \gg 1$. In this case, the bare particle-particle propagator Π_α at $\mathbf{q} = 0$, $\omega = 0$ is small for two particles in different bands. Neglecting this term, we find

$$\Pi_{\alpha=ij} = \int \frac{d^2k}{(2\pi)^2} G_i^{(+)}(\mathbf{k},\epsilon) G_j^{(-)}(-\mathbf{k},\epsilon) = \begin{cases} m_i\tau_i & i = j \\ 0 & i \neq j\,. \end{cases} \tag{43}$$

The calculation reduces to 2×2 matrices with $\ell\ell$ and hh indices only. The mean free time is found in the Born approximation, using Eq. (57), to be

$$\begin{aligned} \frac{1}{\tau_i} &= 2i \sum_{i'} \int \frac{d^2k'}{(2\pi)^2} G^+_{i'}(\mathbf{k}',\epsilon) \left\langle V^2 \right\rangle M_{ii'}(\Delta\theta) M_{i'i}(-\Delta\theta) \\ &= \frac{\left\langle V^2 \right\rangle}{2} \left\{ m_i \left[\left(\xi_H^{(i)}\right)^4 + \left(\xi_L^{(i)}\right)^4 \right] \right. \\ &\quad \left. + m_j \left[\left(\xi_H^{(i)}\xi_H^{(j)}\right)^2 + \left(\xi_L^{(i)}\xi_L^{(j)}\right)^2 \right] \right\}\Big|_{j\neq i}\,. \end{aligned} \tag{44}$$

The following observations simplify the calculation: In the equation for the Cooperon, (40), the disorder line depends on $\Delta\theta = \theta' - \theta$, and Π_β is angle-independent. It is therefore possible to Fourier transform the equation to angular momentum space. Using Eqs. (57) and (42), we note the only nonvanishing terms in $\mathcal{V}_{\alpha\beta}(\Delta\theta) = \sum_m \mathcal{V}^{(m)}_{\alpha\beta} e^{im\Delta\theta}$ have $0 \le m \le 6$.

The Cooperon equation (40) takes the form,

$$C^{(m)}_{\alpha\gamma} = \mathcal{V}^{(m)} + \sum_\beta \mathcal{V}^{(m)}_{\alpha\beta}\Pi_\beta C^{(m)}_{\beta\gamma}\,, \tag{45}$$

where $C_{\alpha\beta}(\theta,\theta') = \sum_m C^{(m)}_{\alpha\beta} e^{im(\theta'-\theta)}$. The Cooperon has a large contribution whenever the matrix $\mathcal{V}^{(m)}_{\alpha\beta}\Pi_\beta$ has an eigenvalue close to 1. This happens for $m = 3$ only, where

$$\mathcal{V}^{(3)} = \frac{\left\langle V^2 \right\rangle}{2} \times \begin{pmatrix} \left(\xi_H^{(\ell)}\right)^4 + \left(\xi_L^{(\ell)}\right)^4 & \left(\xi_H^{(\ell)}\xi_H^{(h)}\right)^2 + \left(\xi_L^{(\ell)}\xi_L^{(h)}\right)^2 \\ \left(\xi_H^{(h)}\xi_H^{(\ell)}\right)^2 + \left(\xi_L^{(h)}\xi_L^{(\ell)}\right)^2 & \left(\xi_H^{(h)}\right)^4 + \left(\xi_L^{(h)}\right)^4 \end{pmatrix}. \tag{46}$$

Since $\Pi_\alpha = 0$ for $\alpha = \ell h$ or $h\ell$, we write $\mathcal{V}^{(3)}$ as a 2×2 matrix with $\ell\ell$ and hh indices only. Using (44), the matrix $\mathcal{V}^{(3)}_{\alpha\beta}\Pi_\beta$ has an eigenvalue 1, with eigenvector $\propto (-\tau_2, \tau_1)$.

We show now that quantum interference corrections lead to weak antilocalization. Using the eigenvector of $\mathcal{V}^{(3)}_{\alpha\beta}\Pi_\beta$, the Cooperon takes the form

$$C(\Delta\theta) = \begin{pmatrix} \tau_2/\tau_1 & -1 \\ -1 & \tau_1/\tau_2 \end{pmatrix} \frac{\left\langle V^2 \right\rangle}{(Dq^2 - i\omega)\tau} e^{i3\Delta\theta}\,. \tag{47}$$

The diffusion constant D, and the mean free time τ, reflect the properties of both bands. In a weak localization diagram, each of the particle lines at one end of the Cooperon is connected with the *other* particle line at the other end of the Cooperon. Because the momenta of the two lines is opposite, $\Delta\theta = \pi$ in the expression for the Cooperon and $e^{i3\Delta\theta} = -1$. This -1 term, which does not exist for the Cooperon in the single-band case, changes the overall sign of the diagram and leads to weak antilocalization.

In the limit of a large band gap we thus find weak antilocalization. We turn now to the opposite limit; a small gap, $\epsilon_g\tau < 1$. In that case we neglect differences in the density of states and scattering times in the two bands, as well as the bulk light hole contribution to the spin overlap functions, $\xi_L^{(i)}$. The calculation is strictly a leading order expansion in k. Here, the Cooperon equation (38) is not reduced to a 2×2 matrix since the propagation of the two Cooperon particles in two different bands should be taken into account. The bare particle-particle propagator at $\mathbf{q} = \omega = 0$ takes the form

$$\Pi = m\tau \begin{pmatrix} 1 & 0 & 0 & 0 \\ 0 & \frac{1}{1+i\epsilon_g\tau} & 0 & 0 \\ 0 & 0 & \frac{1}{1-i\epsilon_g\tau} & 0 \\ 0 & 0 & 0 & 1 \end{pmatrix}, \tag{48}$$

where indices are taken in the order $\ell\ell$, ℓh, $h\ell$, and hh. Although we assume $\epsilon_g\tau \ll 1$, it is necessary to maintain the $\epsilon_g\tau$ terms in Π as they lead to small deviations of the eigenvalues of $\mathcal{V}\Pi$ from unity. Fourier decomposition in angular momentum space of the disorder line, $\mathcal{V}_{\alpha\beta}(\Delta\theta) = \sum_m \mathcal{V}^{(m)}_{\alpha\beta} e^{im\Delta\theta}$, has the following nonvanish-

ing components:

$$\mathcal{V}^{(0)} = \frac{\langle V^2\rangle}{4}\begin{pmatrix}1&1&1&1\\1&1&1&1\\1&1&1&1\\1&1&1&1\end{pmatrix}, \quad (49)$$

$$\mathcal{V}^{(3)} = \frac{\langle V^2\rangle}{2}\begin{pmatrix}1&0&0&-1\\0&1&-1&0\\0&-1&1&0\\-1&0&0&1\end{pmatrix}, \quad (50)$$

$$\mathcal{V}^{(6)} = \frac{\langle V^2\rangle}{4}\begin{pmatrix}1&-1&-1&1\\-1&1&1&-1\\-1&1&1&-1\\1&-1&-1&1\end{pmatrix}. \quad (51)$$

We are interested in eigenvalues of $\Pi\mathcal{V}^{(m)}$ which are close to unity and their corresponding eigenvectors. Calculating $C = (1-\mathcal{V}\Pi)^{-1}\mathcal{V}$, we find the Cooperon

$$\begin{aligned} C(\Delta\theta) = & \quad (52)\\ & \frac{\langle V^2\rangle}{4}\begin{pmatrix}1&1&1&1\\1&1&1&1\\1&1&1&1\\1&1&1&1\end{pmatrix}\frac{1}{(Dq^2-i\omega+\epsilon_g^2\tau/2)\tau}\\ & +\frac{\langle V^2\rangle}{2}\begin{pmatrix}1&0&0&-1\\0&0&0&0\\0&0&0&0\\-1&0&0&1\end{pmatrix}\frac{e^{3i\Delta\theta}}{(Dq^2-i\omega)\tau}\\ & +\frac{\langle V^2\rangle}{2}\begin{pmatrix}0&0&0&0\\0&1&-1&0\\0&-1&1&0\\0&0&0&0\end{pmatrix}\frac{e^{3i\Delta\theta}}{(Dq^2-i\omega+\epsilon_g^2\tau)\tau}\\ & +\frac{\langle V^2\rangle}{4}\begin{pmatrix}1&-1&-1&1\\-1&1&1&-1\\-1&1&1&-1\\1&-1&-1&1\end{pmatrix}\frac{e^{6i\Delta\theta}}{(Dq^2-i\omega+\epsilon_g^2\tau/2)\tau}. \end{aligned}$$

Evidently there are two spin-orbit scattering rates, $\tau_{\rm so}^{-1} = \epsilon_g^2\tau$ and $\epsilon_g^2\tau/2$. When the Cooperon lines are matched in a weak localization diagram, $\Delta\theta = \pi$. Consequently, a -1 term appears in the second and third terms. The -1 factor in the third term is cancelled against another -1 factor appearing due to the contributing matrix elements, $C_{\ell h,h\ell}$ and $C_{h\ell,\ell h}$. The first, third and fourth terms hence generate weak localization while the second term contributes to weak antilocalization. The emerging picture is identical to the one obtained for spin-orbit scattering, where spin singlet states contribute to weak antilocalization while spin triplet states contribute to weak localization.

The calculation of the quantum interference correction to the magnetoconductivity follows the standard route (see, e.g., Refs. 47,66), leading to Eq. (3). This result describes the crossover from weak antilocalization at $\epsilon_g^2\tau\tau_\varphi > 1$ to weak localization at $\epsilon_g^2\tau\tau_\varphi < 1$, as seen in Fig. 8.

C. Model and band structure

In this section we discuss the band structure of a two-dimensional hole gas in a GaAs/AlGaAs heterostructure. This problem was considered theoretically in refs.[34,35]. Here, we present the essential ingredients, relying on the derivation of ref.[34]. Our main purpose is to derive the overlap between spinor wavefunctions in the two bands, which is an important ingredient in the inter-band hole-hole scattering rate calculation.

The lowest bulk valence bands of GaAs are fourfold degenerate at $\mathbf{k}=0$ and split to light and heavy, doubly degenerate bands at finite $\mathbf{k}$. When a confining potential in the $\hat{\mathbf{z}}$ direction is introduced to create the 2DHG, the degeneracy between the bulk light and heavy holes is lifted at $\mathbf{k}=0$ as well. In cases where the confining potential or the lattice lack inversion symmetry, spin-orbit coupling further lifts the twofold degeneracy of each band. The spin-orbit coupling depends on $\mathbf{k}$ thus at finite $\mathbf{k}$, the valence band comprises four bands of different masses and Fermi velocities. Since the splitting between the bulk light and heavy holes is large, the relevant subbands for our experiment are the two originating from the bulk heavy band. We denote these bands as light and heavy but that nomenclature should not be confused with the light and heavy bulk bands.

In the following calculation we use the spherical approximation[69]. Consider the $\mathbf{k}\cdot\mathbf{p}$ Hamiltonian[70] within the spherical approximation, and in the presence of an asymmetric confining potential,

$$H = \left(\gamma_1 + \frac{5\bar{\gamma}}{2}\right)\frac{k^2}{2} - \bar{\gamma}(\mathbf{k}\cdot\mathbf{J})^2 + V(z). \quad (53)$$

Here, $\mathbf{J}$ are the angular momentum matrices for $j=3/2$, and $\gamma_1 = 6.85$ and $\bar{\gamma} = (2\gamma_2+3\gamma_3)/5 = 2.58$ are the Luttinger parameters for GaAs in atomic units. The confining potential $V(z)$ is usually calculated self-consistently within a Hartree approximation[34,35] . Here it is sufficient to assume that $V(z)$ is the result of such a calculation.

A note regarding our notation: The bulk light and heavy holes are denoted by capital letters (L and H). The light and heavy bands originating from the bulk heavy band are denote by ℓ and h. It is the latter two which are relevant for our discussion.

Within the subspace of light and heavy bulk states, and using a $J=\frac{3}{2}$ representation, the two dimensional Hamiltonian takes the form[34,35],

$$H_{\mathbf{k}} = \begin{pmatrix} \epsilon_H^{(0)} + \frac{\gamma_1+\bar{\gamma}}{2}k^2 & i\sqrt{3}\bar{\gamma}Kk_- & -\frac{\sqrt{3}}{2}\bar{\gamma}sk_-^2 & 0 \\ -i\sqrt{3}\bar{\gamma}Kk_+ & \epsilon_L^{(0)} + \frac{\gamma_1-\bar{\gamma}}{2}k^2 & 0 & -\frac{\sqrt{3}}{2}\bar{\gamma}sk_-^2 \\ -\frac{\sqrt{3}}{2}\bar{\gamma}sk_+^2 & 0 & \epsilon_L^{(0)} + \frac{\gamma_1-\bar{\gamma}}{2}k^2 & i\sqrt{3}\bar{\gamma}Kk_- \\ 0 & -\frac{\sqrt{3}}{2}\bar{\gamma}sk_+^2 & -i\sqrt{3}\bar{\gamma}Kk_+ & \epsilon_H^{(0)} + \frac{\gamma_1+\bar{\gamma}}{2}k^2 \end{pmatrix}. \quad (54)$$

Here, $k_\pm \equiv k_x \pm ik_y$. The parameters $s \equiv \langle\psi_L^{(0)}|\psi_H^{(0)}\rangle$, and $iK \equiv \langle\psi_L^{(0)}|k_z|\psi_H^{(0)}\rangle$, where $\psi_H^{(0)}, \psi_L^{(0)}$ are the z-direction states corresponding to the bulk heavy and light holes, respectively reflect the wave function in the third dimension. Note $K \neq 0$ for asymmetric confining potential.

To third order in k the Hamiltonian's eigenvalues are

$$\epsilon_{\mathbf{k}}^{(i)} = \epsilon_H^{(0)} + \left(\frac{\gamma_1+\bar{\gamma}}{2} - \frac{3K^2\bar{\gamma}^2}{\epsilon_L^{(0)} - \epsilon_H^{(0)}}\right)k^2 \pm \frac{3Ks\bar{\gamma}^2}{\epsilon_L^{(0)} - \epsilon_H^{(0)}}k^3, \quad (55)$$

with the upper (lower) sign corresponding to $i = \ell$ ($i = h$). Within this model the two bands are degenerate in the case of a symmetric confining potential ($K = 0$).

The eigenvectors of $H_{\mathbf{k}}$ corresponding to the two relevant bands are $U(\theta)\Xi^{(\ell)}$ and $U(\theta)\Xi^{(h)}$, where

$$U(\theta) = \frac{1}{\sqrt{2}}\begin{pmatrix} 1 & 0 & 0 & 1 \\ 0 & -ie^{-i\theta} & ie^{-i\theta} & 0 \\ 0 & 1 & 1 & 0 \\ -ie^{3i\theta} & 0 & 0 & ie^{3i\theta} \end{pmatrix}. \quad (56)$$

the angle θ marks the direction of $\mathbf{k}$ in the x-y plane (this transformation is a single valued version of the unitary transformation used in ref. 34), $\Xi^{(\ell)}(\mathbf{k}) = \left(\xi_H^{(\ell)}(k), -e^{2i\theta}\xi_L^{(\ell)}(k), 0, 0\right)$ and $\Xi^{(h)}(\mathbf{k}) = \left(0, 0, e^{2i\theta}\xi_L^{(h)}(k), \xi_H^{(h)}(k)\right)$. Here $\xi_{L,H}^{(i)}$ are chosen to be real, and the dependence upon the direction of $\mathbf{k}$ is given explicitly in the expressions for $\Xi^{(i)}(\mathbf{k})$. The ξ's, depending only on the magnitude of $\mathbf{k}$, may be explicitly calculated, but are not needed here. For our calculation we need the overlap of the spin part of two different eigenstates of the system, as a function of the two momenta directions. This overlap is given by

$$M_{ij}(\mathbf{k},\mathbf{k}') = \xi^{\dagger(i)}(\mathbf{k})U^\dagger(\theta)U(\theta')\xi^{(j)}(\mathbf{k}') \quad (57)$$

$$= \begin{cases} \frac{1}{2}\left(1 + e^{3i\Delta\theta}\right)\xi_H^{(i)}(k)\xi_H^{(i)}(k') \\ \qquad + \frac{1}{2}\left(e^{i\Delta\theta} + e^{2i\Delta\theta}\right)\xi_L^{(i)}(k)\xi_L^{(i)}(k') & i = j, \\ \frac{1}{2}\left(1 - e^{3i\Delta\theta}\right)\xi_H^{(i)}(k)\xi_H^{(j)}(k') \\ \qquad + \frac{1}{2}\left(e^{i\Delta\theta} - e^{2i\Delta\theta}\right)\xi_L^{(i)}(k)\xi_L^{(j)}(k') & i \neq j, \end{cases}$$

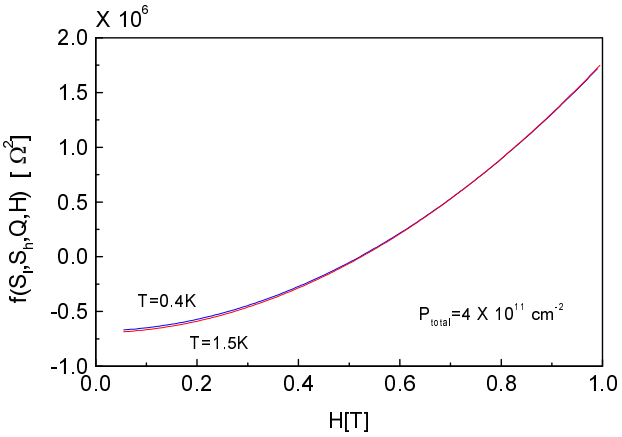

FIG. 25: $f(S_l, S_h, Q, H)$ vs. magnetic field at two different temperatures for $p_{total} = 4 \times 10^{11} cm^{-2}$.

where $\Delta\theta = \theta' - \theta$, and the indices i and j take the value ℓ or h. This result is used in the calculation of the transport properties in Section (V A 2).

Acknowledgments

We thank I. L. Aleiner, B. L. Altshuler, A. M. Finkel'stein, B. I. Halperin, A. Kamenev, D. L. Maslov, B. N. Narozhny, A. Punnoose, and M. Reznikov for stimulating discussions. This work was supported by the Israeli science foundation and by German-Israeli DIP grant.

APPENDIX A

The function $f(S_l, S_h, Q, H)$ in Eq. (1) is given by

$$f(S_l,S_h,Q,H) = \frac{1}{[1+(H/W)^2]^2}\cdot\frac{1}{(S_l+S_h+2Q)^4}\cdot \left[C_0 + C_1\cdot H^2 + C_2\cdot H^4 + C_3\cdot H^6\right],$$

where

$$C_0 = -(S_l+S_h+2Q)^2\cdot(S_lS_h - Q^2)^2,$$

$$
\begin{aligned}
C_1 &= Q_0 + Q\cdot Q_1 + Q^2\cdot Q_2 + Q^3\cdot Q_3 + Q^4\cdot Q_4,\\
C_2 &= P_0 + Q\cdot P_1 + Q^2\cdot P_2,\\
C_3 &= R_l^2 R_h^2 (R_l+R_h)^2,
\end{aligned}
$$

and

$$
\begin{aligned}
Q_0 &= (R_h S_l^2 + R_l S_h^2)^2 - 2(S_l+S_h)(R_h^2 S_l + R_l^2 S_h) S_l S_h,\\
Q_1 &= 4\left[(S_l-S_h)(R_h^2 S_l^2 - R_l^2 S_h^2) + 2R_l R_h S_l S_h (S_l+S_h)\right],\\
Q_2 &= 2\left[S_l S_h (R_l+R_h)^2 + R_l R_h (S_l-S_h)^2 \right.\\
&\quad \left. + 4(R_h S_l + R_l S_h)^2\right],\\
Q_3 &= 8(R_h^2 S_l + R_l^2 S_h),\\
Q_4 &= R_l^2 - 6R_l R_h + R_h^2,\\
P_0 &= 2R_l^2 R_h^2 (S_l - S_h)^2 - (R_h^2 S_l - R_l^2 S_h)^2\\
&\quad + 2R_l R_h (R_h^2 S_l^2 + R_l^2 S_h^2),\\
P_1 &= 4R_l R_h [R_h S_l (R_l + 2R_h) + R_l S_h (R_h + 2R_l)],\\
P_2 &= 2R_l R_h (R_h^2 + R_l^2).
\end{aligned}
$$

Fig. 25 depicts $f(S_l, S_h, Q, H)$ vs. magnetic field at $T = 0.4$ and $1.5K$ for $p_{total} = 4\times 10^{11} cm^{-2}$.

---

* Present address: Laboratory of Atomic and Solid State Physics, Cornell University, Ithaca, NY 14853.

† Present address: Department of Physics, Princeton University, Princeton, NJ 08544.

[1] S. V. Kravchenko, G. V. Kravchenko, J. E. Furneaux, V. M. Pudalov, and M. D'Iorio, Phys. Rev. B **50**, 8039 (1994).

[2] E. Abrahams, P. W. Anderson, D. C. Licciardello, and T. V. Ramakrishnan, Phys. Rev. Lett. **42**, 673 (1979).

[3] A. M. Finkel'stein, Zh. Eksp. Teor. Fiz. **84**, 168 (1983) [Sov. Phys.-JETP **57**, 97 (1983)]; A. M. Finkel'stein, Z. Phys. A **56**, 189 (1984); C. Castellani *et al.*, Phys. Rev. B **30**, 1596 (1984); C. Castellani, C. DiCastro, P. A. Lee, and M. Ma, Phys. Rev. B **30**, 527 (1984); C. Castellani, C. Di Castro, and P. A. Lee, Phys. Rev. B **57**, R9381 (1998).

[4] S. V. Kravchenko, W. E. Mason, G. E. Bowker, J. E. Furneaux, V. M. Pudalov, and M. D'Iorio, Phys. Rev. B **51**, 7038 (1995); S. V. Kravchenko, D. Simonian, M.P. Sarachik, W. Mason, and J. E. Furneaux, Phys. Rev. Lett. **77**, 4938 (1996); D. Popović, A. B. Fowler, and S. Washburn, Phys. Rev. Lett. **79**, 1543 (1997); R. Heemskerk and T. M. Klapwijk, Phys. Rev. B **58**, R7154 (1998).

[5] P. T. Coleridge, R. L. Williams, Y. Feng, and P. Zawadzki, Phys. Rev. B **56**, R12764 (1997); J. Lam, M. D'Iorio, D. Brown, and H. Lafontaine, Phys. Rev. B **56**, R12741 (1997).

[6] S. J. Papadakis and M. Shayegan, Phys. Rev. B **57**, R15068 (1998).

[7] Y. Hanein, D. Shahar, J. Yoon, C. C. Li, D. C. Tsui, and H. Shtrikman, Phys. Rev. B **58**, R13338 (1998).

[8] E. Ribeiro, R. D. Jäggi, T. Heinzel, K. Ensslin, G. Medeiros-Ribeiro, and P. M. Petroff, Phys. Rev. Lett. **82**, 996 (1999).

[9] Y. Hanein, U. Meirav, D. Shahar, C. C. Li, D. C. Tsui and H. Shtrikman, Phys. Rev. Lett. **80**, 1288 (1998).

[10] M. Y. Simmons, A. R. Hamilton, M. Pepper, E. H. Linfield, P. D. Rose and D. A. Ritchie, Phys. Rev. Lett. **80** 1292 (1998).

[11] S. J. Papadakis, E. P. De Poortere, H. C. Manoharan, M. Shayegan, and R. Winkler, Science **283**, 2056 (1999).

[12] Y. Yaish, O. Prus, E. Buchstab, S. Shapira, G. Ben Yosef, U. Sivan, and A. Stern, Phys. Rev. Lett. **84**, 4954 (2000).

[13] P. Phillips, Y. Wan, I. Martin, S. Kngsh, and D. Dalidovich, Nature **395**, 253 (1998); D. Belitz and T. R. Kirkpatrick, Phys. Rev. B **58**, 8214 (1998).

[14] Q. Si and C. M. Varma, Phys. Rev. Lett. **81**, 4951 (1998).

[15] S. Chakravarty, S. Kivelson, C. Nayak, and K. Völker, Phil. Mag. B **79**, 859 (1999).

[16] V. Dobrosavljević, E. Abrahams, E. Miranda, and S. Chakravarty, Phys. Rev. Lett. **79**, 455 (1997); D. Simonian, S. V. Kravchenko, M. P. Sarachik, and V. M. Pudalov, Phys. Rev. B **57**, R9420 (1998).

[17] A. R. Hamilton, M. Y. Simmons, M. Pepper, E. H. Linfield, P. D. Rose and D. A. Ritchie, Phys. Rev. Lett. **82**, 1542 (1999).

[18] S. S. Safonov, S. H. Roshko, A. K. Savchenko, A. G. Pogosov, and Z. D. Kvon, Phys. Rev. Lett. **86**, 272 (2001).

[19] S. J. Papadakis, E. P. De Poortere, M. Shayegan, and R. Winkler, Phys. Rev. Lett. **84**, 5592 (2000); S. J. Papadakis, E. P. De Poortere, and M. Shayegan, Phys. Rev. B **62**, 15373 (2000).

[20] O. Prus *et al.,* (2000) unpublished.

[21] X. G. Feng, D. Popović, and S. Washburn, Phys. Rev. Lett. **83**, 368 (1999)

[22] S. He and X. C. Xie, Phys. Rev. Lett. **80**, 3324 (1998).

[23] B. L. Altshuler and D. Maslov, Phys. Rev. Lett. **82**, 145 (1999).

[24] A. Gold and V. T. Dolgopolov, Phys. Rev. B **33**, 1076 (1986); S. Das Sarma and E. H. Hwang, Phys. Rev. Lett. **83**, 164 (1999).

[25] A. R. Hamilton, M. Y. Simmons, M. Pepper and D. A. Ritchie, Aust. J. Phys. **53**, 523 (2000).

[26] V. M. Pudalov, Pis'ma Zh. Eksp. Teor. Fiz. **66**, 168 (1997).

[27] Y. Meir, Phys. Rev. Lett. **83**, 3506 (1999); Y. Meir, Phys. Rev. B **61,** 16470 (2000).

[28] N. W. Ashcroft and D. D. Mermin, *Solid State Physics*, Harcourt Brace College Publishers (1976), p. 240.

[29] V. F. Gantmakher and Y.B. Levinson, Sov. Phys. JETP, **47**, 133 (1978).

[30] E. Zaremba, Phys. Rev. B **45**, 14143 (1992).

[31] H. L. Stormer, Z. Schlesinger, A. Chang, D. C. Tsui, A. C. Gossard, and W. Wiegmann, Phys. Rev. Lett. **51**, 126 (1983).

[32] J. P. Eisenstein, H. L. Stormer, V. Narayanamurti, A. C. Gossard, and W. Wiegmann, Phys. Rev. Lett. **53**, 2579 (1984).

[33] J. P. Lu, J. B. Yau, S. P. Shukla, M. Shayegan, L. Wissinger, U. Rössler, and R. Winkler, Phys. Rev. Lett. **81**, 1282 (1998).

[34] D. A. Broido and L. J. Sham, Phys. Rev. B **31**, 888 (1985).

[35] U. Ekenberg and M. Altarelli, Phys. Rev. B **32**, 3721 (1985).

[36] G. Goldoni and F. M. Peeters, Phys. Rev. B **51**, 17806 (1995).

[37] R. Winkler, S. J. Papadakis, E. P. De Poortere, and M.

Shayegan, Phys. Rev. Lett. **84**, 713 (2000); R.Winkler, cond-mat/0002003.
[38] S. S. Murzin, S. I. Dorozhkin, G. Landwehr, and A. C. Gossard, JETP Lett. **67**, 113 (1998).
[39] For a review, see B. L. Altshuler and A. G. Aronov, *Electron Electron Interactions in Disordered Systems*, edited by M. Pollak and A. L. Efros (North Holland, Amsterdam, 1984).
[40] M. A. Paalanen, D. C. Tsui, and J. C. M. Hwang, Phys. Rev. Lett. **51**, 2226 (1983).
[41] K. K. Choi, D. C. Tsui, and S. C. Palmateer, Phys. Rev. B **33**, 8216 (1986).
[42] Y. Hanein, D. Shahar, J. Yoon, C. C. Li, D. C. Tusi and H. Shtrikman, Phys. Rev. B **58**, R7520 (1998).
[43] M. Y. Simmons, A. R. Hamilton, M. Pepper, E. H. Linfield, P. D. Rose and D. A. Ritchie, Phys. Rev. Lett. **84**, 2489 (2000).
[44] P. D. Dresselhaus, C. M. A. Papavassiliou, R. G. Wheeler and R. N. Sacks, Phys. Rev. Lett. **68**, 106 (1992).
[45] W. Knap, C. Skierbiszewski, A. Zduniak, E. Litwin-Staszewska, D. Bertho, F. Kobbi, J. L. Robert, G. E., Pikus, F. G. Pikus, S. V. Iordanskii, V. Mosser, K. Zekentes, and Yu. B. Lyanda-Geller, Phys. Rev. B **53**, 3912 (1996).
[46] Y. Lyanda-Geller, Phys. Rev. Lett. **80**, 4273 (1998).
[47] N. S. Averkiev, L. E. Golub and G. E. Pikus, JETP. **86**, 780 (1998).
[48] M. I. D'yakonov and V. I. Perel', Zh. Eksp. Teor. Fiz. **60**, 1954 (1971) [Sov. Phys. JETP **33**, 1053 (1971)].
[49] S. Pedersen, C. B. Sorensen, A. Kristesen, P. E. Lindelof, L. E. Golub and N. S. Averkiev, Phys. Rev. **60**, 4880 (1999).
[50] H. Fukuyama, J. Phys. Soc. Jpn. **50**, 3407 (1981).
[51] A. M. Finkel'stein, Zh. Eksp. Teor. Fiz. **84**, 168 (1983) [Sov. Phys.-JETP **57**, 97 (1983)].
[52] H. Fukuyama, Y. Isawa, and H. Yasuhara, J. Phys. Soc. Jpn. **52**, 16 (1983).
[53] P. A. Lee and T. V. Ramakrishnan, Phys. Rev. B**26**, 4009 (1982).
[54] B. L. Altshuler, A. G. Aronov, A. I. Larkin, and D. E. Khmelnitskii, Zh. Eksp. Teor. Fiz. **81**, 768 (1981) [Sov. Phys.-JETP **54**, 411 (1981)].
[55] G. Bergmann, Phys. Rev. B **25**, 2937 (1982); Phys. Rev. Lett. **48**, 1046 (1982); Z. Phys. B **48**, 5 (1982).
[56] R. A. Davies and M. Pepper, J. Phys. C **16**, L353 (1983).
[57] G. Brunthaler, A. Prinz, G. Bauer, V. M. Pudalov, E. M. Dizhur, J. Jaroszynski, P. Glod and T. Dietl, Ann. Phys.-Berlin **8**, 579 (1999).
[58] P. T. Coleridge, A. S. Sachrajda and P. Zawadzki, cond-mat/9912041.
[59] U. Meirav, M. Heiblum and F. Stern, Appl. Phys. Lett. B **52**, 1268 (1988).
[60] S. C. Dultz and H. W. Jiang, Phys. Rev. Lett. **84**, 4689 (2000).
[61] Y. Yaish, O. Prus, E. Buchstab, G. Ben Yosef, and U. Sivan, unpublished (2001); Y. Yaish, Ph.D. Thesis, Technion-IIT (2001) pp. 88-95.
[62] S. Ilani, A. Yacoby, D. Mahalu and H. Shtrikman, Phys. Rev. Lett. **84**, 3133 (2000).
[63] G. Zala, B. N. Narozhny, and I. L. Aleiner, cond-mat/0105406. See also Y. Y. Proskuryakov, A. K. Savchenko, S. S. Safonov, M. Pepper, M. Y. Simmons, and D. A. Ritchie, cond-mat/0109261.
[64] K. Flensberg and B. Y.-K. Hu, Phys. Rev. Lett. **73**, 3572 (1994); Phys. Rev. B **52**, 14796 (1995).
[65] Y. Yaish, unpublished (2001).
[66] S. Hikami, A. I. Larkin, and Y. Nagaoka, Prog. Theor. Phys. **63**, 707 (1980).
[67] D. Rainer and G. Bergmann, Phys. Rev. B **32**, 3522 (1985).
[68] I. V. Gornyi, A. P. Dmitriev, and V. Yu. Kachorovskii, Pis'ma Zh. Éksp. Teor. Fiz. **68**, 314 (1998) [JETP Lett. **68**, 338 (1998)].
[69] A. Baldereschi and N. O. Lipari, Phys. Rev. B **8**, 2697 (1973).
[70] J. M. Luttinger, Phys. Rev. **102**, 1030 (1956).